Ore Geology Reviews 90 (2017) 166–183

Contents lists available at ScienceDirect

Ore Geology Reviews

journal homepage: www.elsevier.com/locate/oregeorev

Ophiolitic chromitites from the Kızılyüksek area of the Pozantı-Karsantı ophiolite (Adana, southern Turkey): Implication for crystallization from a fractionated boninitic melt

Erdi Avcı [a], İbrahim Uysal [a,*], Recep Melih Akmaz [b], Samet Saka [a]

[a] Department of Geological Engineering, Karadeniz Technical University, 61080 Trabzon, Turkey
[b] Department of Geological Engineering, Bülent Ecevit University, 67100 Zonguldak, Turkey

ARTICLE INFO

Article history:
Received 17 April 2016
Accepted 29 August 2016
Available online 30 August 2016

Keywords:
Kızılyüksek chromitites
Pozantı-Karsantı ophiolite
Southern Turkey
Platinum-group element and mineral
Silicate inclusions
Island arc

ABSTRACT

Ophiolitic rocks are widely distributed in Turkey. One type, the Pozantı-Karsantı ophiolite from southern Turkey, contains a large number of chromitite deposits located mostly in the mantle peridotites and close to the Moho transition zone dunite and cumulate dunites. Cr-spinel grains from the chromitites are represented by high Cr# [100 × Cr / (Cr + Al) = 68–81], and their Mg# [100 × Mg / (Mg + Fe^{2+})] range from 54 to 71. Gallium and Co contents vary between 18 and 32 ppm and 185–266 ppm, respectively, and they show negative correlation with Cr#. A detailed optical investigation reveals that the Cr-spinel grains contain silicate, platinum-group mineral (PGM) and base metal sulfide (BMS) inclusions. Single phase inclusions of amphibole are the only hydrous silicate phases in the investigated chromitites, and they contain low TiO_2 (<0.43 wt.%). Olivine, with high Fo (~96) and NiO contents (0.48–0.68 wt.%), and clinopyroxene, with low TiO_2 (<0.1 wt.%), Al_2O_3 (<2.84 wt.%) and Na_2O contents (<0.4 wt.%) were also observed as primary silicate inclusions. Chromitites contain low concentrations of total platinum-group elements (PGE) ranging between 32 and 162 ppb, with an average value of 93 ppb. Primitive mantle-normalized PGE diagrams show almost flat to positive slopes from Os to Rh (Rh_N/Os_N = 0.99 to 8.5) and negative slope from Rh to Pt and Pd. All samples show marked positive Ru anomalies. Consistent with the geochemical data, Ru, Os, and Ir bearing PGE sulfide (laurite-erlichmanite solid solution series [(Ru, Os)S_2–(Os, Ru)S_2] phases) are the most common PGM detected in the investigated chromitite samples. They show a narrow range of Os-Ru substitution [Ru#; Ru/(Ru + Os) = 0.72–0.97], indicating no erlichmanite in the PGM paragenesis. In addition to the most common PGM laurite, several osmium (Os, Ir), iridium (Ir, Os), irarsite, and one single grain of speryllite ($PtAs_2$) were detected as magmatic inclusions in Cr-spinel. Three unknown PGE/PGE–BME (base metal element) phases were also detected in Cr-spinel grains with compositions that correspond to the chemical formulas of (Os, Ru, Ir, Rh, Fe, Pd)$_2S_5$, Ir(Rh,Pt,Ni,Cu)S_3, and (Ir, Rh, Ru)$_2$(Ni, Cu)S_3, respectively. The high Cr# and low Ti content of Cr-spinel grains and amphibole inclusions with low Ti content as hydrous phases in Cr-spinel grains require a hydrous melt depleted in incompatible trace elements for the formation of investigated chromitites; therefore, we suggest a fore arc tectonic environment for the generation of Kızılyüksek chromitites. The presence of Os-Ir alloys and Ru-rich laurites implies that Cr-spinel crystallization took place at relatively high temperature (1100–1300 °C) and low $f(S_2)$ (between −1 and −3) conditions. Major and trace element compositional variations of Cr-spinel, wide variation of Rh_N/Os_N ratios of the chromitites and depletion of Os in the chromitites compared to Ir and Ru may imply that Kızılyüksek chromitites crystallized from a variously fractionated boninitic melt.

1. Introduction

Ophiolitic rocks are widely exposed across the globe. The mantle peridotites that make up the bottom part of the ophiolitic rock assemblage are very important for understanding the nature of petrological processes such as melting and melt-rock interactions during the formation of oceanic crust, as well as for the economically important chromitites they contain. How ophiolitic chromitite is formed is still a matter of debate. The first model proposed for the formation of podiform chromitite involved deposition of Cr-spinel crystals from the primary melts circulating continuously in magmatic channels within the mantle (Lago et al., 1982; Leblanc and Ceuleneer, 1992). Later studies have also shown that the interaction of melt with mantle peridotites plays an important role in forming podiform chromitites (Arai and Yurimoto, 1994; Zhou and Robinson, 1994; Zhou et al., 1996, 1998; Arai, 1997). In addition,

* Corresponding author.
E-mail address: uysal.ibrahim@gmail.com (İ. Uysal).

http://dx.doi.org/10.1016/j.oregeorev.2016.08.033
0169-1368/

the tectonic settings of ophiolitic chromitites are also under debate. The Cr# [100 × Cr / (Cr + Al)] values for the Cr-spinel that form the ophiolitic chromitites indicate tectonic settings for chromitites in which they formed (Dick and Bullen, 1984; Kamenetsky et al., 2001 and references therein). Back-arc basin environments, which are represented by a low degree of partial melting, have been proposed as possible environments for chromitites that contain Al-rich Cr-spinel crystals (Al-rich chromitites; Cr# < 60), while arc-front arc settings, which are represented by a high degree of partial melting, have been suggested as environments for chromitites that contain Cr-rich Cr-spinel crystals (Cr-rich chromitites; Cr# > 60) (Uysal et al., 2007b, 2009b; González-Jiménez et al., 2011; Zaccarini et al., 2011; Garuti et al., 2012; Akmaz et al., 2014; Zhou et al., 2014).

In recent studies, ophiolitic chromitites have also been a focus due to the presence of platinum-group elements (PGE: Os, Ir, Rh, Rh, Pt, Pd), which have great economic value (e.g., Fischer et al., 1988; Ferrario and Garuti, 1988; Orberger et al., 1988; Distler et al., 2008; El Ghorfi et al., 2008). Their concentrations in the mantle are controlled by sulfide or alloy phases rather than silicate phases, while concentrations in chromitites are generally controlled by platinum-group mineral (PGM) inclusions within Cr-spinel crystals. Iridium-group platinum-group elements (IPGE: Os, Ir, Ru) are compatible and therefore prefer to stay in residual phases during partial melting and tend to crystallize together with early solid phases during crystallization from a melt. On the other hand, palladium-group platinum-group elements (PPGE: Rh, Pt, Pd) have a rather incompatible nature and prefer to be in the melt phase during partial melting (Leblanc, 1991; Bockrath et al., 2004; Ahmed et al., 2009; Uysal et al., 2009b). The properties of these elements reveal important information about the petrological evolution of mantle rocks and chromitites.

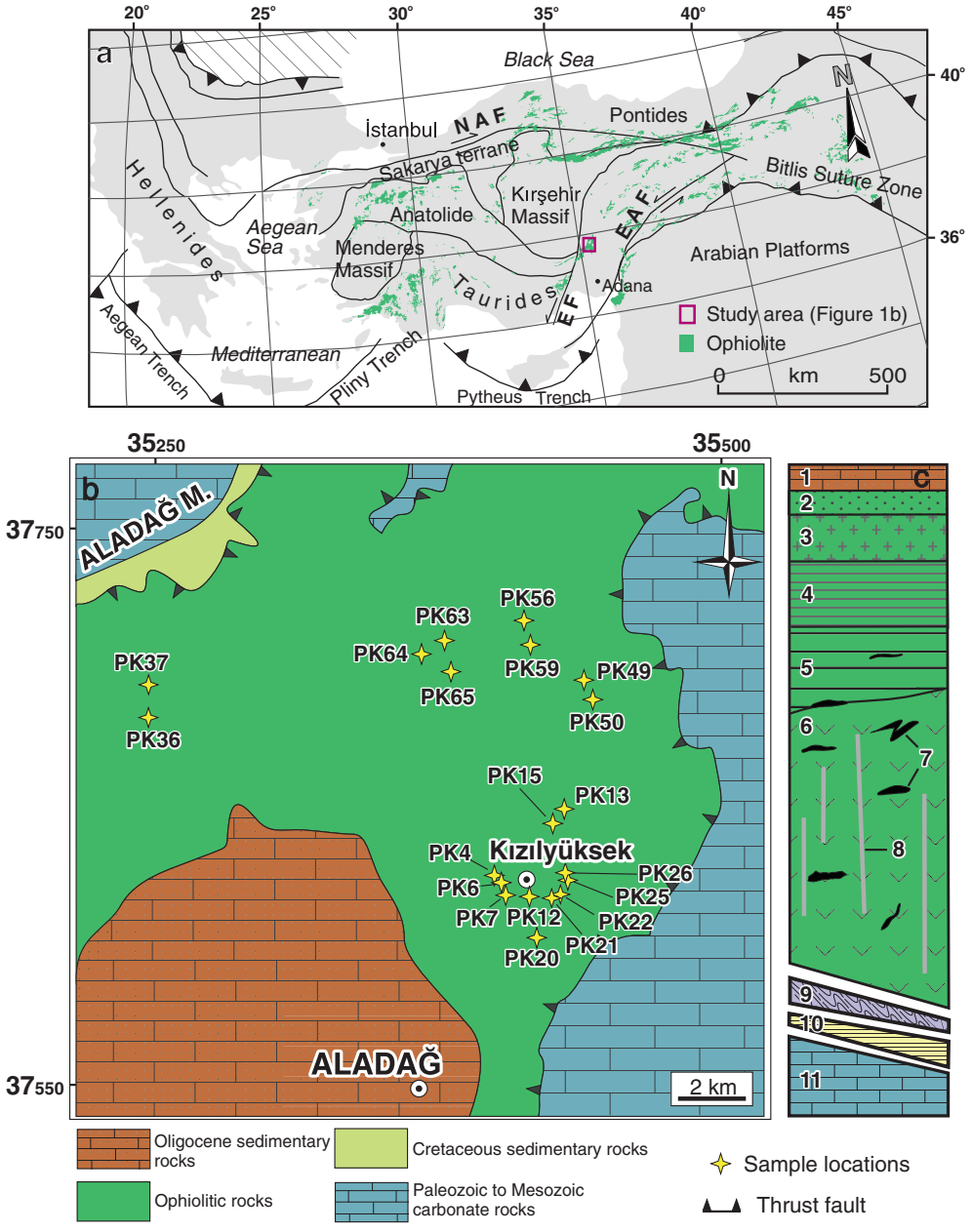

Fig. 1. a: Main tectonic units of Turkey (Dinter, 1988) and distributions of ophiolitic rocks in Turkey (MTA, 2002). NAF: North Anatolian Fault, EAF: East Anatolian Fault, EF: Ecemiş Fault. b: Simplified geological map of the study area (after MTA, 2002). c: Representative columnar section for the Pozantı-Karsantı ophiolite that contains the Kızılyüksek chromitites (from Bingöl, 1978; Çakır, 1978; Çataklı, 1978; Çapan, 1980; Tekeli, 1981). 1: sedimentary rocks, 2: isotropic gabbros, 3: mafic cumulates, 4: pyroxenites, 5: cumulate dunites with banded chromitites, 6: mantle peridotites, 7: podiform chromitites, 8: diabase dykes, 9: metamorphic sole (amphibolite), 10: ophiolitic melange, 11: autochthonous units.

The ophiolitic rocks in Turkey have a wide distribution, and the Pozantı-Karsantı ophiolitic sequence is one of these rock assemblages. In this sequence, chromitites are associated mostly with harzburgite and dunite-type mantle peridotites as well as cumulate dunites. Chromitites, in association with mantle peridotites of the ophiolitic sequence, are massive in appearance and have a partly disseminated texture, while chromitites associated with cumulate dunites are mostly banded. Cr-spinel crystals with Cr# values ranging from 68 to 81 contain both platinum-group mineral (PGM) inclusions and base metal sulfide (BMS) inclusions. These phases in Cr-spinel crystals yield important information about the physiochemical conditions of chromitites (Ahmed and Arai, 2002, 2003; Augé et al., 2002; Uysal et al., 2009a, 2009b, 2015; Akmaz et al., 2014).

Saka et al. (2014) stated that the Kızılyüksek region of the Pozantı-Karsantı ophiolite is comprised of mantle peridotites and overlying crustal rocks, and that mantle peridotites are residues of 22% to 26% partial melting of primitive mantle under various pressure conditions. In this study, we investigated the major and trace element composition of Cr-spinel as well as the composition of PGM, base metal mineral (BMM) and silicate inclusions in Cr-spinel crystals of chromitites from the Kızılyüksek region. In addition, we determined whole-rock PGE contents of the studied chromitites. The results were evaluated in terms of the tectonic setting of the chromitites and the petrological processes that governed their formation because the PGE display very different behaviour during partial melting and differentiation and are important for determining the degree of differentiation of the melts that crystallize the chromitites.

2. Regional geology

Turkey is geologically divided into three main tectonic units: the Pontides, the Anatolides and the Taurides (Dilek and Moores, 1990; Okay, 2008). The Pozantı-Karsantı ophiolite, which is widely exposed between the towns of Pozantı and Karsantı (Aladağ), and which was first named by Bingöl (1978), is located in the Tauride geologic belt at the north of the city of Adana (Fig. 1a).

The Ecemiş fault, which has a left-lateral strike-slip character, separates the Pozantı-Karsantı ophiolite and the underlying Aladağ platform consisting of extensively deformed Paleozoic-Early Mesozoic carbonate rocks (Tekeli et al., 1984) at the west of the Bolkar massif and ophiolitic rocks (Dilek and Moores, 1990). The mélange and the Aladağ platform are tectonically overlain by the northeast-southwest-extending Pozantı-Karsantı ophiolite of the upper Cretaceous age (Juteau, 1980; Dilek and Moores, 1990) (Fig. 1b). The Upper Triassic and lower Cretaceous carbonate rocks of the Aladağ platform are unconformably overlain by chaotic olistostromal mélange that contains ophiolitic fragments (Tekeli et al., 1984). With regard to rock type, structural properties and position, the Aladağ ophiolite sequence is comprised of three units: the ophiolitic mélange at the bottom, the metamorphic slice above the mélange, and a peridotite nappe at the top that hosts the Kızılyüksek chromitites (Bingöl, 1978; Çakır, 1978; Çataklı, 1978; Çapan, 1980; Tekeli, 1981) (Fig. 1c). The ophiolitic sequence hosting the Kızılyüksek chromitites starts at its bottom with porphyroclastic tectonic textured harzburgites, granoblastic harzburgites, and mantle tectonites that are cut by isolated diabase dykes; continues with ultramafic cumulates of dunite and pyroxenite and mafic cumulates (Bingöl, 1978; Çakır, 1978; Çataklı, 1978; Juteau, 1979; Çapan, 1980) (Fig. 1c).

3. Podiform chromitites

Podiform chromitites associated with the Pozantı-Karsantı ophiolite mostly occur within harzburgite and dunite-type rocks as massive (Fig. 2a), disseminated (Fig. 2b), banded (Fig. 2c), and rarely, nodular and vein type ore bodies (Fig. 2d). Chromitite bodies that are mostly surrounded by dunites generally show sharp transitions to these rocks, but in some cases, there is a gradual change represented by a decrease in Cr-spinel modal abundances from massive chromitites to disseminated chromitites and towards dunites. Chromitites, particularly those in the mantle part of the ophiolitic sequence, are characterized by massive and disseminated textures, while those close to crustal rocks or within the cumulate dunites are mostly banded.

The Kızılyüksek chromitites are generally massive (>80% Cr-spinel) (Fig. 3a) and semi- massive (60–75% Cr-spinel) (Fig. 3b, c) textured. Disseminated chromitites (Fig. 3d), found mostly in the upper mantle part of the ophiolitic sequence as well as in the cumulate dunites, are composed of euhedral Cr-spinel crystals in a modal abundance of 20–60%. Banded chromitites, particularly those in the cumulate dunites, are composed of Cr-spinel crystals with a modal abundance of 50–75% and alternation of fresh olivine crystals (Fig. 3e). Nodular chromitites,

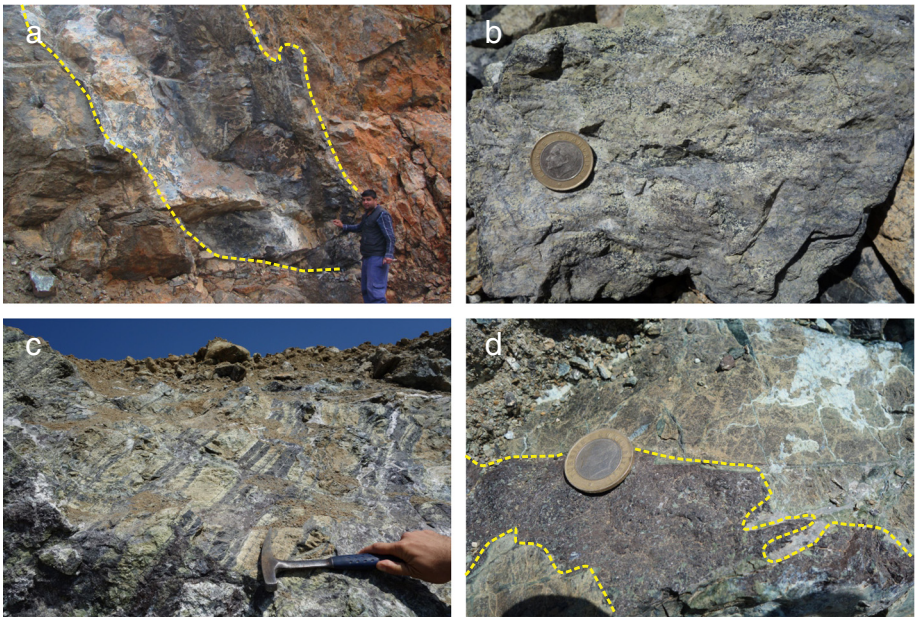

Fig. 2. Massive and semi-massive chromitite within harzburgite (a), disseminated chromitites with relatively fresh olivine crystals (b), banded chromitites in the ultramafic cumulates (c), vein of massive chromitites hosted by serpentinized dunite (d).

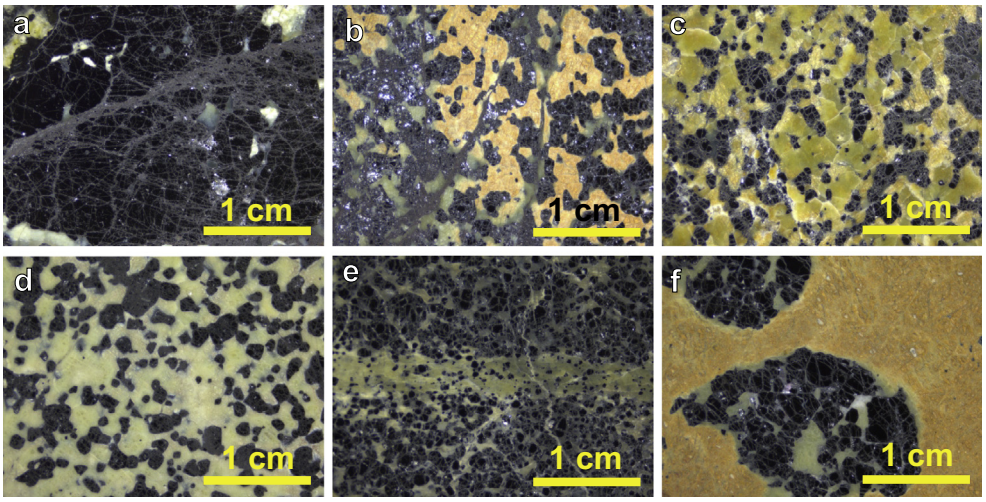

Fig. 3. Massive chromitite sample with abundant fractures and cracks (a); semi-massive chromitite sample with ~65% modal Cr–spinel abundance within mostly serpentinized matrix (b); disseminated chromitite samples with ~40% modal Cr-spinel abundance having fresh (c) and partly serpentinized (d) silicate matrix; banded chromitite sample comprised of relatively fresh olivine and abundant Cr–spinel layers (e), and nodular chromitite sample containing ~1 cm in diameter nodules within highly serpentinized matrix (f).

which are observed only in mantle peridotites, are made up of Cr-spinel crystals that have a modal abundance of about 50% and show signs of tectonic deformation. The nodules of Cr-spinel crystals are mostly filled by serpentinized olivine minerals (Fig. 3f). Cr-spinel crystals from the massive and semi-massive chromitites are usually fractured and brecciated (Fig. 4a, b). Cr-spinel crystals that fragmented as a result of tectonic deformation create the cataclastic texture (Fig. 4b), and this phenomenon is commonly observed in the Kızılyüksek chromitites. The matrix that fills the space between fractured and cracked Cr-spinels of massive and semi-massive chromitites is generally serpentinized. However, the matrix in the disseminated chromitites is comprised of olivine and serpentine minerals (Fig. 4c). Almost all the chromitite samples that were petrographically examined were composed of fresh Cr-spinel crystals, and in some cases, alteration was significant along the margins and fractures of the crystals. In the Back Scattered Electron (BSE) images, this alteration is easily recognized by its brighter appearance compared to fresh Cr-spinel crystals (Fig. 4d).

4. Samples and analytical methods

Forty-two chromitite samples that have different textures and are located in mantle and close to or above the Moho transition zone of the Pozantı-Karsantı ophiolite have been taken from 20 different locations. Electron-probe micro-analyses (EPMA) were performed on each chromitite sample to obtain the chemical composition of Cr-spinel crystals of the chromitites. Two polished blocks were prepared from each chromitite sample, and the surfaces of each polished block were scanned under reflected light at 250–500× magnification to detect tiny mineral inclusions such as PGM, BMM and silicate inclusions enclosed by Cr-spinel crystals. Platinum-group minerals (PGM) were

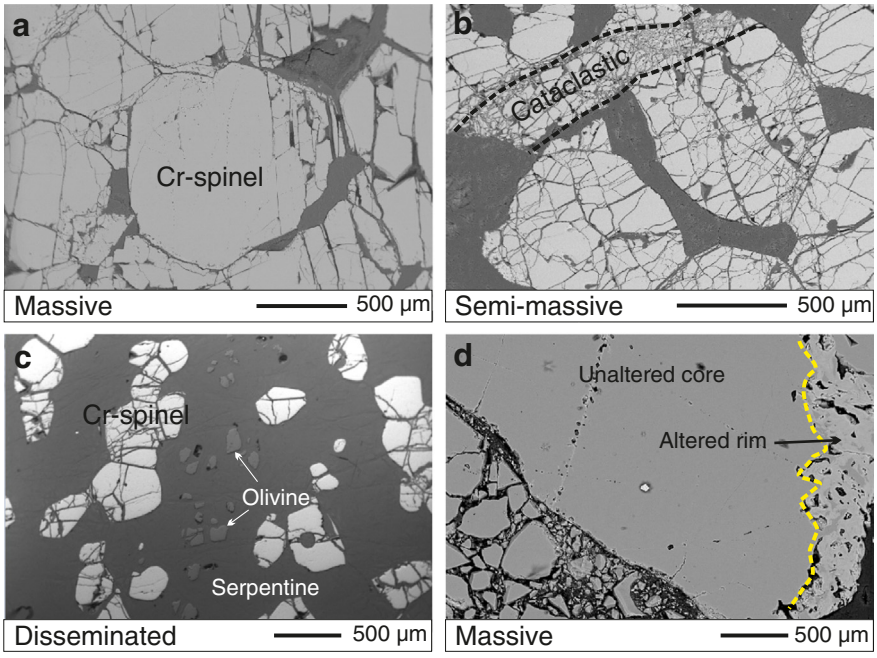

Fig. 4. Back scattered electron images of the Kızılyüksek chromitites. Massive chromitite with subhedral Cr-spinel grains (a), semi-massive chromite sample showing cataclastic texture with highly cracked Cr-spinel crystals (b), disseminated chromite sample composed of relatively altered and fresh olivine matrix and Cr-spinel crystals (c), massive chromite sample containing Cr-spinel crystals altered through crack and rim (d).

Table 1
Average composition of fresh and altered Mg–chromite crystals of high–Cr chromitites from the Kızılyüksek. Cr# = 100×Cr / (Cr + Al), Mg# = 100×Mg / (Mg + Fe^{2+}), N: Number of spot analysis, bdl: below detection limit, MCA: Modal Chromite Abundance, D: Disseminated, M: Massive, SM: Semi–massive, B: Banded, N: Nodular, *: parental melt composition, AAC: Analysed area of chromite crystals.

Sample#	PK4-1	PK6	PK7	PK12B	PK13B	PK13-1	PK15	PK20	PK20B	PK21	PK22	PK22B	PK25	PK25B	PK26	PK26B	PK26-1	PK36	PK37	PK37B	PK37-1	PK49	PK49B	PK50
Texture	D	D	D	D	SM	SM	D	D	D	D	M	M	D	D	M	M	M	M	B	B	B	D	D	D
MCA	~20%	~35%	~50%	~55%	~60%	~65%	~40%	~30%	~30%	~35%	~95%	~95%	~25%	~35%	~95%	~90%	~95%	~80%	~75%	~75%	~75%	~40%	~40%	~45%
N	5	5	5	5	5	4	3	5	5	5	5	2	5	4	5	3	4	3	5	5	3	5	5	4
AAC	Core	Core	Core	Core	Core	Core	Core	Core	Core	Core	Core	Core	Core	Core	Core	Core	Core	Core	Core	Core	Core	Core	Core	Core
TiO_2	0.17	0.23	0.19	0.20	0.21	0.19	0.19	0.17	0.16	0.22	0.21	0.22	0.27	0.26	0.17	0.17	0.16	0.17	0.15	0.17	0.16	0.24	0.24	0.21
Al_2O_3	9.67	12.77	11.37	11.34	12.51	12.26	10.23	10.29	10.04	12.59	13.63	13.82	13.93	13.58	16.21	16.84	16.57	10.23	10.21	10.23	10.44	10.71	10.71	10.95
Cr_2O_3	60.19	57.80	59.92	59.37	58.98	56.94	59.30	59.56	60.74	58.09	58.57	57.42	54.12	55.16	54.57	53.39	51.65	58.59	61.13	60.86	59.81	59.93	59.93	58.56
Fe_2O_3	1.63	2.34	1.80	2.19	2.17	3.19	3.53	2.67	2.04	2.33	1.76	2.64	1.19	2.62	2.34	3.09	2.99	4.52	2.18	2.14	2.36	2.37	2.37	2.52
FeO	16.75	14.15	14.10	14.91	13.57	12.27	12.41	14.92	15.66	13.20	11.66	11.12	15.02	13.95	12.54	12.42	11.77	12.54	13.82	14.39	13.96	14.77	14.77	13.49
MnO	0.15	bdl	bdl	bdl	bdl	0.06	bdl	bdl	bdl	bdl	bdl	bdl	0.12	bdl	bdl	bdl	0.03	bdl	bdl	bdl	0.04	bdl	bdl	bdl
NiO	bdl	0.09	0.09	0.05	0.07	0.07	0.14	0.02	0.04	0.13	0.13	0.20	0.06	0.10	0.13	0.14	0.17	0.06	0.07	0.05	0.08	0.09	0.09	0.03
MgO	10.88	13.21	13.07	12.60	13.69	13.99	13.81	12.32	11.94	13.71	14.96	15.23	11.90	13.04	14.54	14.73	14.45	13.82	13.17	12.80	12.87	12.65	12.65	13.13
Σ	99.45	100.59	100.55	100.66	101.19	98.96	99.61	99.96	100.64	100.27	100.92	100.65	96.61	98.71	100.50	100.78	97.78	99.94	100.73	100.64	99.72	100.75	100.75	98.90
Mg#	54	62	62	60	64	67	66	60	58	65	70	71	59	63	67	68	69	66	63	61	62	60	60	63
Cr#	81	75	78	78	76	76	80	80	80	76	74	74	72	73	69	68	68	79	80	80	79	79	79	78
Al_2O_3*	10.79	12.24	11.64	11.62	12.13	12.03	11.08	11.12	10.99	12.17	12.58	12.65	12.69	12.56	13.48	13.68	13.60	11.08	11.07	11.08	11.19	11.32	11.32	11.44
TiO_2*	0.27	0.35	0.29	0.31	0.32	0.30	0.30	0.27	0.26	0.33	0.32	0.33	0.39	0.38	0.27	0.27	0.26	0.27	0.25	0.28	0.25	0.35	0.35	0.33
FeO/MgO*	–	–	–	–	–	–	–	–	–	–	0.63	0.59	–	–	0.73	0.72	0.69	0.67	–	–	–	–	–	–

Table 1 *(continued)*

Sample#	PK50B	PK50-1-2	PK50-2-1	PK50-2-2	PK55-1	PK56	PK56B	PK56-2	PK59	PK59B	PK63	PK63B	PK63-1	PK63-2	PK64	PK64-2	PK65	PK15	PK22B	PK36	PK50B	PK59
Texture	SM	B	D	D	M	M	M	M	M	M	SM	SM	SM	SM	N	N	M	D	M	M	SM	M
MCA	~65%	~50%	~55%	~55%	~85%	~85%	~85%	~85%	~90%	~90%	~75%	~75%	~75%	~75%	~60%	~60%	~85%	~40%	~95%	~80%	~65%	~90%
N	4	3	5	5	5	4	5	5	3	4	3	5	4	5	5	2	5					
AAC	Core	Core	Core	Core	Core	Core	Core	Core	Core	Core	Core	Core	Core	Core	Core	Core	Core	Rim-Crack	Rim-Crack	Rim-Crack	Rim-Crack	Rim-Crack
TiO_2	0.20	0.19	0.20	0.19	0.18	0.17	0.19	0.19	0.18	0.18	0.18	0.16	0.15	0.16	0.16	0.17	0.17	0.20	0.23	0.16	0.20	0.18
Al_2O_3	10.96	10.31	10.68	10.63	11.23	10.67	10.65	10.43	11.27	11.56	9.66	10.11	10.00	9.81	10.31	9.83	10.52	9.96	13.33	9.90	10.98	11.33
Cr_2O_3	58.48	58.61	57.55	57.04	56.30	58.48	60.68	57.94	57.06	57.80	59.19	60.99	59.06	59.16	61.35	60.78	60.21	58.70	55.91	57.50	58.29	55.95
Fe_2O_3	0.42	3.97	3.40	3.64	3.89	4.13	2.39	3.41	3.68	3.40	2.60	1.84	2.82	2.55	1.60	2.18	2.47	6.02	4.65	6.36	3.83	8.49
FeO	14.66	12.42	12.23	12.08	13.17	12.15	13.57	12.81	13.70	13.55	14.42	14.80	14.09	13.71	14.74	14.55	14.48	10.61	10.23	11.76	12.38	11.25
MnO	0.18	0.03	0.10	0.09	0.13	bdl	bdl	0.09	0.17	bdl	bdl	bdl	0.15	0.11	bdl	0.09	bdl	0.00	0.00	0.00	0.00	0.18
NiO	0.03	0.14	0.06	0.11	0.05	0.07	0.02	0.08	0.07	bdl	0.08	bdl	0.03	0.03	0.07	0.06	0.10	0.00	0.12	0.00	0.00	0.00
MgO	11.35	13.75	13.58	13.57	13.05	14.09	13.47	13.27	12.87	13.34	12.22	12.49	12.50	12.66	12.63	12.48	12.76	15.27	15.69	14.33	14.02	15.22
Σ	96.27	99.43	97.80	97.35	97.99	99.77	100.97	98.21	99.00	99.83	98.35	100.39	98.81	98.21	100.86	100.12	100.70	100.78	100.17	100.00	99.70	102.61
Mg#	57	66	66	67	64	67	64	65	63	64	60	60	61	62	60	60	61	72	73	69	67	71
Cr#	78	79	78	78	77	79	79	79	77	77	80	80	80	80	80	81	79	80	74	80	78	77
Al_2O_3*	11.44	11.12	11.31	11.28	11.57	11.30	11.29	11.18	11.59	11.72	10.78	11.02	10.97	10.87	11.12	10.87	11.23	10.94	12.46	10.91	11.45	11.62
TiO_2*	0.31	0.30	0.31	0.30	0.28	0.28	0.29	0.30	0.28	0.28	0.28	0.25	0.25	0.26	0.26	0.27	0.27	0.31	0.35	0.26	0.31	0.28
FeO/MgO*	–	–	–	–	0.77	0.65	0.77	0.73	0.82	0.78	–	–	–	–	–	–	–	–	0.51	0.60	–	0.54

detected and marked in 22 out of 84 polished blocks. Although few chromitite samples were found to contain BMM inclusions, silicate inclusions were detected in almost all polished blocks. Three chromitite samples with different chemical composition were selected to obtain the trace element contents of Cr-spinel crystals. Moreover, 14 chromitite samples taken from different levels of the ophiolitic suite and having various chemical composition were selected for their whole rock platinum-group element (PGE) concentrations.

In situ micro-chemical analyses of Cr-spinel, PGM, BMM and silicate inclusions were performed using a CAMECA SX-100 electron-probe micro-analyser (EPMA) in the Department of Earth and Environmental Sciences at Ludwig Maximilian University of Munich, Germany. Analytical conditions for quantitative WDS analyses were 15–20 kV accelerating voltage, 20 nA probe current, and a beam diameter of 1 μm. For the Cr-spinel and silicate inclusions, calibrations were carried out using natural and synthetic reference materials: andradite for Ca, Si, and Fe; corundum for Al; periclase for Mg; rutile for Ti; albite for Na; orthoclase for K; chromite for Cr; and NiO for Ni. The Fe^{2+} and Fe^{3+} contents of the Cr-spinels were calculated on the basis of spinel stoichiometry (XY_2O_4). Detection limits (wt.%) of the elements measured for the Cr-spinel and silicate inclusions were 0.06 for SiO_2, TiO_2, CaO, and Na_2O; 0.04 for K_2O; 0.05 for Al_2O_3; 0.09 for Cr_2O_3; 0.1 for FeO and NiO; 0.08 for MnO; and 0.07 for MgO. The PGM and base metal minerals (BMM) were first qualitatively examined by energy dispersion spectrometry (EDS) and then analysed quantitatively by wavelength-dispersion spectrometry (WDS). Pure metals were used as standards for PGE, Ni and Cu, arsenopyrite was used for As, and pyrite was used for Fe. Various X-ray lines were used in the analyses: Lα for Ru, Ir, Rh and Pt; Mα for Os; Lα for Pd and As; and Kα for S, Ni, Fe and Cu. For the PGE and BME, the detection limits were 0.09 for Os; 0.13 for Ir; 0.23 for Ru, Rh, and Pt; 0.03 for S; 0.25 for Pd; 0.06 for Ni; 0.07 for Fe; and 0.02 for Cu and As.

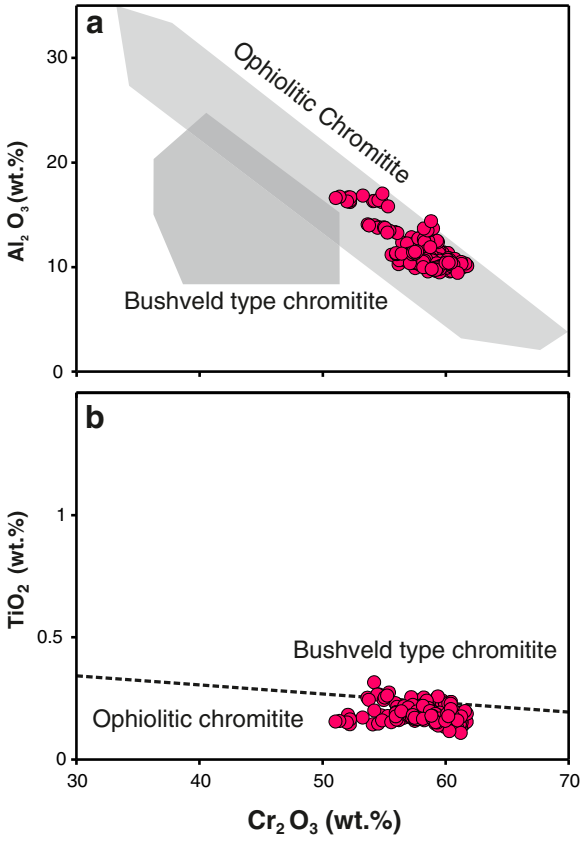

Fig. 5. Composition of Mg-chromite plotted on Al_2O_3 versus Cr_2O_3 (a) and TiO_2 versus Cr_2O_3 (b) diagrams. Ophiolitic and Bushveld type chromitite fields are from Bonavia et al. (1993).

The trace element contents of some Cr-spinel crystals, the major oxide composition of which has already been determined, were analysed by a Thermo X-Series 2 quadrupole ICP-MS coupled to a New Wave UP-213 Laser Ablation system at Geochemistry/ICP-MS Laboratory at the School of Earth and Ocean Sciences, University of Victoria, Victoria, BC, Canada. The signal for each element was normalized to an internal standard (aluminium) correcting for ablation efficiency and instrumental drift. NIST 611 glass was used to calibrate the signal. Quality of calibration was confirmed by re-analysis of NIST 611 after every four shots. The method of ICP-MS analysis for the trace elements of Cr-spinel crystals has been described in Akmaz et al. (2014).

The selected chromitite samples were analysed for the full suite of whole rock PGE using a nickel sulfide fire-assay pre-concentration method followed by ICP-MS at Genalysis Laboratory, Perth, Western Australia, following the method described by Chan and Finch (2001). Detection limits were 2 ppb for Os, Ir, Ru, Pt, and Pd, and 1 ppb for Rh.

5. Geochemistry of Kızılyüksek chromitites

5.1. Cr-spinel major oxide composition

Major oxide composition of the Cr-spinels from chromitites were mostly obtained from the core, which is the least altered part of the crystals. In some samples, point analysis was also done along fractures and cracks where alteration was partly or significantly apparent. Table 1 shows the results. For the analysis of the central part of the Cr-spinel crystals, Cr_2O_3 content varies from 51.65 to 61.35 wt.%, and Al_2O_3 concentrations are in the range of 9.66 to 16.84 wt.%. Fe_2O_3 contents of the Cr-spinel crystals are from 0.42 to 4.52 wt.%, and TiO_2 concentrations are from 0.15 to 0.27 wt.% (Table 1). Cr_2O_3 and Al_2O_3 contents of the altered parts along the fractures, cracks and margins of the Cr-spinel crystals of Kızılyüksek chromitites are 55.91–58.70 and 9.90–13.33 wt.%, respectively, and Fe_2O_3 and TiO_2 contents are up to 8.49 and 0.23 wt.%, respectively (Table 1).

The Cr# values are between 68 and 81, and the Mg# values vary in a wider range, from 54 to 71. Disseminated chromitites with relatively lower Cr-spinel/silicate matrix ratios are represented by Cr-spinels with lower Mg# values, while massive chromitites with higher Cr-spinel modal abundances have higher Mg# values. For Cr-spinel phases, Cr# values of >65 indicate that such chromitites are high-Cr chromitites (Leblanc and Violette, 1983; Dick and Bullen, 1984), and Mg# and Cr# values of >50 are indicative of "Mg-chromite" composition (Stevens, 1944). Cr_2O_3 contents of Mg-chromite crystals from the Kızılyüksek chromitites decrease with increasing Al_2O_3 content (Fig. 5a). In some chromitite samples, TiO_2 contents of Mg-chromites show a slight increase with decreasing Cr_2O_3 concentrations, although TiO_2 and Cr_2O_3 contents of most Mg-chromite do not show any significant relationship to one another (Fig. 5b).

Table 2
Some minor and trace element concentrations (ppm) and Cr# values of Mg–chromite grains from the Kızılyüksek chromitites. bdl: below detection limit.

Element	Cr#	Ni	Mn	Ti	V	Zn	Co	Ga	Sc
Detection Limits		10.7	4.7	2	1.1	0.6	0.3	0.4	8
PK20	79	498	1378	826	620	361	259	19	bdl
PK20	80	510	1389	829	626	353	258	18	bdl
PK20	80	520	1433	846	642	376	266	20	bdl
PK26B	68	1067	964	928	949	348	189	32	bdl
PK26B	68	1107	958	882	942	359	190	30	bdl
PK26B	68	1135	943	902	937	367	185	32	bdl
PK59B	77	624	1332	990	676	353	227	20	8
PK59B	77	586	1368	991	685	338	230	20	bdl
PK59B	77	573	1444	1043	699	345	237	21	bdl
Mean		***75***	***736***	***1246***	***915***	***753***	***356***	***227***	***24***

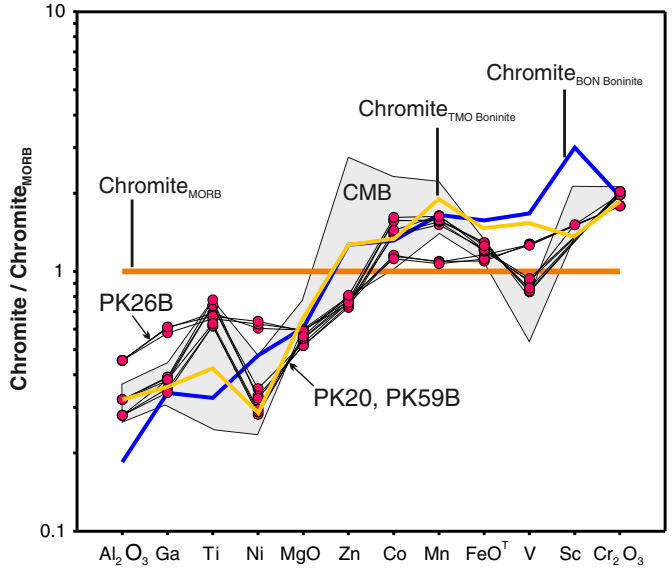

Fig. 6. Cr-spinel$_{MORB}$ normalized major and trace elements patterns of Mg-chromite crystals from the Kızılyüksek chromitites. Cr-spinel$_{MORB}$, TMO and BON boninites data sources are taken from Page and Barnes (2009). BON: Bonin Island, TMO: Thetford Mines Ophiolite, CMB: Caribou Mountain block podiform chromitites.

5.2. Trace element composition of Mg-chromite

The average Ni, Mn, Ti, V, Zn, Co and Ga concentrations of the Mg-chromites that are represented by high-Cr contents are 736, 1246, 915, 753, 356, 227 and 24 ppm, respectively (Table 2). Fig. 6 shows a multi-element diagram in which some major and trace element values for the Mg-chromite crystals of Kızılyüksek chromitites are normalized by the values seen in Cr-spinels from mid-ocean ridge basalts (MORB). Al, Ga, Ti, Ni, Mg and Zn concentrations of the studied Mg-chromite crystals are depleted compared to those of the Cr-spinel crystals from MORB, while Co, Mn, Fe and Cr elements show relative enrichment (Fig. 6). In samples PK59B and PK20, vanadium is partly depleted with respect to the Cr-spinels from MORB, but the V concentration in sample PK26B is represented by a slight enrichment. The Mg-chromite crystals in sample PK26B are partly enriched in Al, Ga, Ni and V with respect to samples PK59B and PK20, while Co and Mn contents are relatively depleted (Fig. 6).

Comparison of trace element concentrations in the Mg-chromite crystals of the studied chromitite samples with the Cr# values of the Mg-chromites reveals decreasing concentrations of Ni, V and Ga with increasing Cr# values, while Co and Mn concentrations are increased with increasing Cr# (Fig. 7).

5.3. Whole-rock platinum-group element (PGE) geochemistry

The whole-rock total PGE contents of the Kızılyüksek chromitites are very low, ranging from 32 to 162 ppb (avg: 93 ppb). IPGE abundances of these chromitites (23–141 ppb) are higher than PPGE abundances (8–55 ppb) ($PPGE_N/IPGE_N = 0.24–0.76$), and chromitites are represented with Pd/Ir ratios usually below 0.74 (Table 6). In some samples of Kızılyüksek chromitites, Ir and Ru abundances are relatively depleted with respect to ophiolitic chromitites from various parts of the world. In contrast to the Ir abundances, the Os abundances of all studied samples show significant depletion (Fig. 11). In primitive mantle normalized PGE plots, most samples display a positive slope from Os to Ru. Ru-Rh variations in samples differ somewhat. Some samples show a negative slope from Ru to Rh, Pt and Pd, while some display a flat

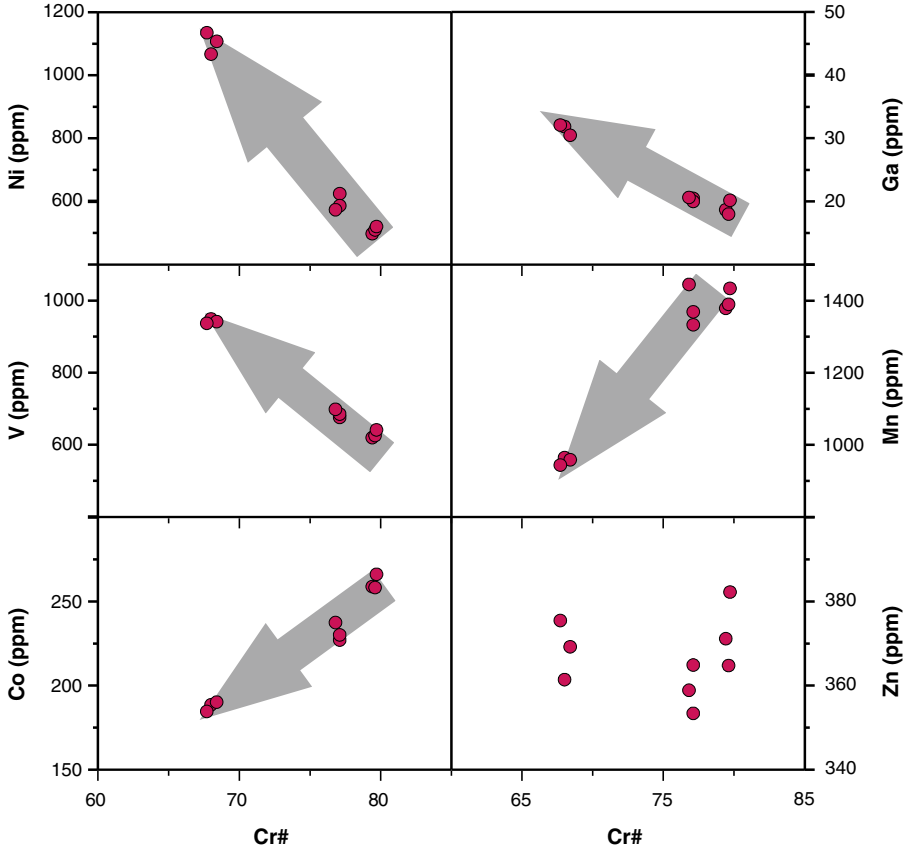

Fig. 7. Relationship between some trace elements content and Cr# values of Mg-chromite crystals from the Kızılyüksek chromitites.

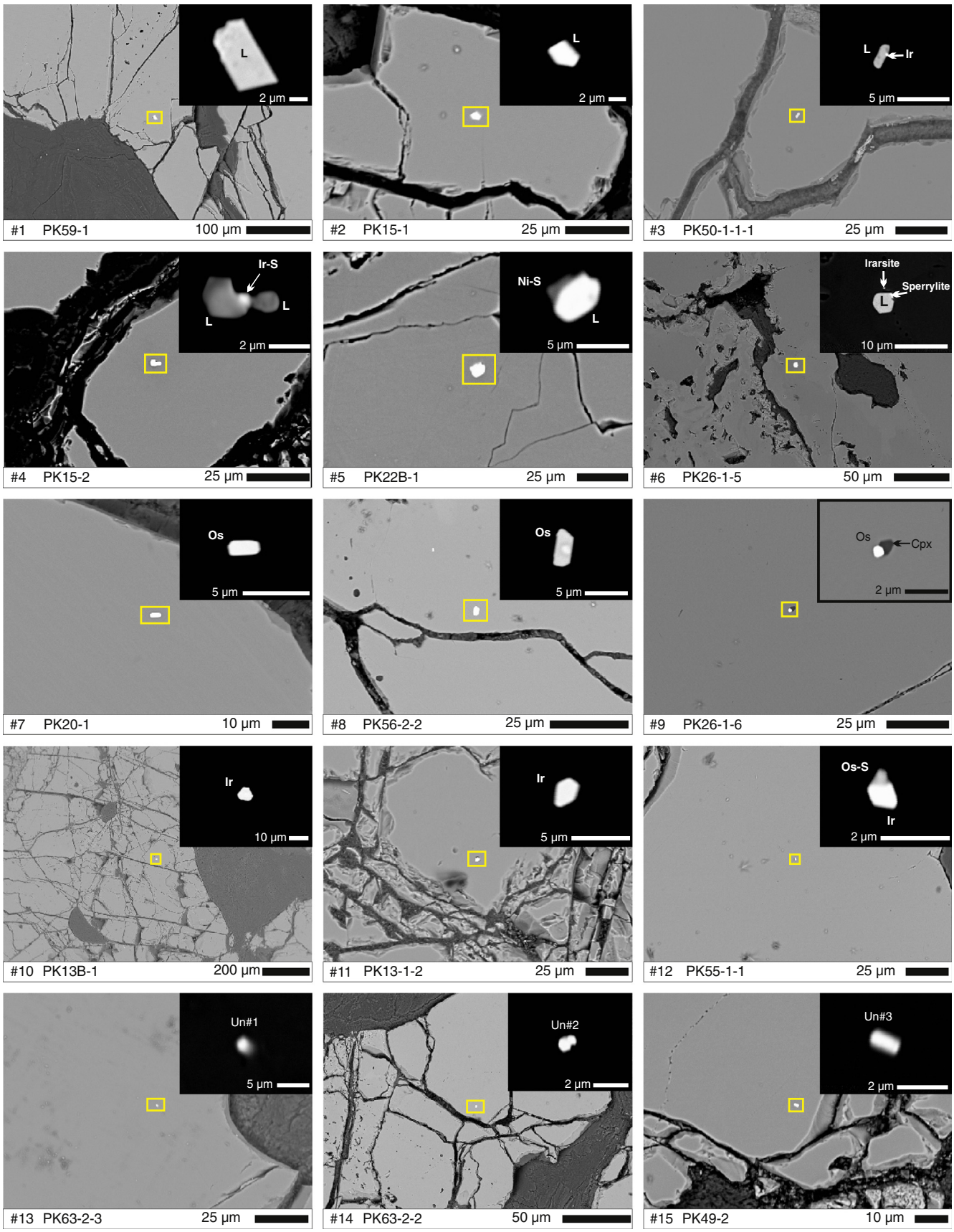

Fig. 8. BSE images showing textural and morpholigical relations of single and polyphase PGM inclusions in Mg-chromite crystals from the Kızılyüksek chromitites. Insets in each figures show the focused image obtained by higher contrast. L: Laurite, Ir-S: Iridium-sulfur phase, Ni-S: Nickel-sulfur phase, Ir: Iridium, Os: Osmium, Cpx: Clinopyroxene, Os-S: Osmium-sulfur phase, Un#: Unidentified phase. The last number in the samples' names indicate inclusion number labeled during the analyses.

Table 3
Representative electron microprobe analyses of PGM's in Mg–chromite grains (Fig. 8) from the Kızılyüksek chromitites. L: Laurite, bdl: below detection limit, Ir: Iridium, Os: Osmium, Spry: Sperrylite, Un#: Unidentified phase, Ru# = Ru/(Ru + Os).

Sample#	PK4-1	PK13-1	PK15	PK15	PK22B	PK26-1	PK50-1-1	PK50-2-1	PK56-2	PK59	PK65	PK20	PK26-1	PK56-2	PK56-2	PK13B	PK13-1	PK50-2-1	PK26-1	PK63-2	PK63-2	PK49
Inclusion#	1	1	1	2	1	5b	1	1	1	1	1	1	6	2	3	1	2	2	5a	3	2	2
Fig. 8, #	–	–	2	4	5	6	3	–	–	1	–	7	9	8	–	10	11	23	6	13	14	15
Mineral	L	L	L	L	L	L	L	L	L	L	L	Os	Os	Os	Os	Ir	Ir	Ir	Spry	Un#1	Un#2	Un#3
Os	24.50	12.40	11.46	18.20	13.22	21.34	10.68	3.55	19.15	11.41	5.01	53.25	61.55	46.80	51.54	30.23	29.70	34.82	0.20	43.65	0.12	0.17
Ir	8.25	4.86	6.76	9.03	4.50	8.60	5.97	3.27	8.01	11.06	5.70	41.51	37.30	40.80	43.40	68.49	63.88	58.59	bdl	11.87	50.93	44.28
Ru	33.90	46.79	43.40	37.57	44.80	33.93	43.94	52.84	37.77	39.95	52.36	3.29	0.90	11.74	3.52	0.42	4.62	bdl	0.25	9.68	bdl	2.93
Rh	bdl	bdl	1.53	0.70	0.10	1.85	0.57	0.77	0.28	1.55	0.60	0.33	0.12	0.58	0.52	0.36	0.22	0.10	0.12	1.28	8.03	17.50
Pt	0.43	0.42	bdl	0.35	0.48	0.35	0.42	0.18	0.34	bdl	0.05	0.05	bdl	bdl	bdl	bdl	0.50	bdl	57.24	bdl	5.24	bdl
Pd	bdl	bdl	0.80	bdl	bdl	bdl	bdl	bdl	bdl	0.64	0.74	bdl	bdl	bdl	0.65	bdl	bdl	5.95	bdl	0.16	bdl	bdl
Ni	bdl	bdl	bdl	bdl	0.77	bdl	1.00	0.66	bdl	0.10	0.21	0.98	bdl	0.57	bdl	0.10	bdl	bdl	0.08	bdl	1.13	6.49
Fe	bdl	0.08	bdl	bdl	0.13	bdl	0.08	0.21	bdl	0.23	bdl	bdl	bdl	bdl	0.12	0.17	0.84	0.17	bdl	0.13	bdl	bdl
Cu	bdl	bdl	bdl	bdl	0.09	bdl	0.05	bdl	bdl	0.04	0.04	bdl	bdl	bdl	bdl	0.02	0.05	bdl	bdl	bdl	9.24	6.43
S	33.56	35.78	35.37	34.54	35.04	33.14	34.50	37.15	33.65	35.22	35.45	bdl	bdl	bdl	bdl	bdl	bdl	bdl	0.22	32.08	24.82	20.53
As	bdl	bdl	0.02	bdl	bdl	0.87	bdl	bdl	bdl	bdl	bdl	bdl	bdl	bdl	0.04	bdl	bdl	0.16	42.36	bdl	bdl	bdl
∑	100.65	100.33	99.34	100.39	99.14	100.07	97.21	98.63	99.20	100.20	100.15	99.42	99.87	100.21	99.79	99.78	99.81	99.80	100.47	98.85	99.51	98.32
Os	0.248	0.117	0.109	0.179	0.126	0.216	0.104	0.032	0.192	0.110	0.047	0.504	0.582	0.465	0.512	0.300	0.281	0.346	0.004	1.144	0.002	0.004
Ir	0.083	0.045	0.063	0.088	0.043	0.086	0.057	0.029	0.080	0.106	0.053	0.389	0.349	0.401	0.427	0.674	0.598	0.576	0.000	0.308	1.007	1.060
Ru	0.646	0.830	0.775	0.696	0.806	0.646	0.803	0.901	0.714	0.725	0.918	0.059	0.016	0.220	0.066	0.008	0.082	0.000	0.008	0.477	0.000	0.133
Rh	0.000	0.000	0.027	0.013	0.002	0.035	0.010	0.013	0.005	0.028	0.010	0.006	0.002	0.011	0.010	0.007	0.004	0.002	0.004	0.062	0.296	0.782
Pt	0.004	0.004	0.000	0.003	0.004	0.003	0.004	0.002	0.003	0.000	0.000	0.000	0.000	0.000	0.000	0.000	0.005	0.000	1.009	0.000	0.102	0.000
Pd	0.000	0.000	0.014	0.000	0.000	0.000	0.000	0.000	0.000	0.011	0.012	0.000	0.000	0.000	0.011	0.000	0.000	0.106	0.000	0.008	0.000	0.000
Ni	0.000	0.000	0.000	0.000	0.024	0.000	0.032	0.019	0.000	0.003	0.006	0.030	0.000	0.018	0.000	0.003	0.000	0.000	0.005	0.000	0.073	0.509
Fe	0.000	0.002	0.000	0.000	0.004	0.000	0.002	0.007	0.000	0.008	0.000	0.000	0.000	0.000	0.004	0.006	0.027	0.006	0.000	0.012	0.000	0.000
Cu	0.000	0.000	0.000	0.000	0.003	0.000	0.001	0.000	0.000	0.001	0.001	0.000	0.000	0.000	0.000	0.001	0.001	0.000	0.000	0.000	0.553	0.465
∑ metal	0.984	0.999	0.988	0.982	1.012	0.988	1.013	1.003	0.996	0.991	1.047	0.988	0.950	1.115	1.030	0.998	0.998	1.036	1.031	2.011	2.033	2.953
S	2.016	2.001	1.992	2.018	1.988	1.989	1.987	1.997	2.004	2.015	1.959	0.000	0.000	0.000	0.000	0.000	0.000	0.000	0.024	4.989	2.942	2.946
As	0.000	0.000	0.000	0.000	0.000	0.022	0.000	0.000	0.000	0.000	0.000	0.000	0.000	0.000	0.001	0.000	0.000	0.004	1.945	0.000	0.000	0.000
∑ anion	2.016	2.001	1.992	2.018	1.988	2.012	1.987	1.997	2.004	2.015	1.959	0.000	0.000	0.000	0.001	0.000	0.000	0.004	1.969	4.989	2.942	2.946
∑	3.000	3.000	2.979	3.000	3.000	3.000	3.000	3.000	3.000	3.006	2.980	0.988	0.950	1.115	1.031	0.998	0.998	1.040	3.000	7.000	4.976	5.892
Ru#	0.72	0.88	0.88	0.80	0.86	0.75	0.89	0.97	0.79	0.87	0.95	–	–	–	–	–	–	–	–	–	–	–

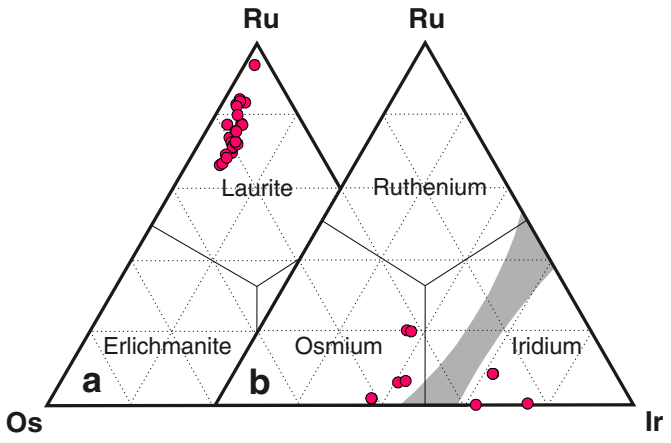

Fig. 9. Ternary diagrams showing classification of a: laurites and b: Os-Ir alloys obtained in Mg-chromite crystals from the Kızılyüksek chromitites.

pattern from Ru to Rh, and a negative slope from Rh to Pt and Pd. However, in some samples, there is a positive slope from Ru to Rh that is uncharacteristic of ophiolitic chromitites. Like other samples, these samples also show a negative slope from Rh to Pt and Pd. The Pd contents of the studied samples are very low; except for three samples, the concentrations are below the detection limit of 2 ppb. The Pd contents of two samples in particular show enrichment rather than a sharp negative slope from Rh to Pt (Fig. 11). As an overall assessment, the Os-Rh patterns of the samples are quite variable, and primitive mantle normalized Rh/Os ratios (Rh_N/Os_N) are in the range of 0.99 to 8.5 (Table 6).

5.4. Inclusions within Mg-chromite crystals

5.4.1. Platinum-group mineral (PGM) inclusions

The Mg-chromite crystals contain euhedral-subhedral PGM inclusions (mostly primary inclusions) of <10 μm in size (Fig. 8). These inclusions within the Kızılyüksek chromitites are mostly represented by laurite of ~2–10 μm size. These phases within fresh Mg-chromite crystals distant from fractures are mostly euhedral and single-phase (Fig. 8 #1–2) but also form multi-phases with other PGM (Ir and Ir-S) (Fig. 8 #3–4) and BMS (Ni-S) (Fig. 8 #5). Ru and Os contents of the laurites are 33.9 to 52.84 wt.% and 3.55 to 24.5 wt.%, respectively. Ir, Rh and Pt concentrations are 3.27 to 9.51 wt.%, <1.85 wt.% and <0.85 wt.%, respectively (Table 3). The laurite crystals of these chromitites are enriched in Ru compared to Os with a Ru# [Ru / (Ru + Os)] values ranging between 0.72 and 0.97 (Fig. 9a).

In addition to laurite, osmium and iridium were found as primary alloys with sizes of 2 to 8 μm (Fig. 8 #7–12), and these phases were evaluated in the Ru-Os-Ir triangular diagram (Fig. 9b). Osmium crystals within fresh Mg-chromite crystals are generally found to be single-phase (Fig. 8 #7–8). However, in rare cases, two-phase inclusions of osmium-clinopyroxene were also observed (Fig. 8 #9). Like osmium crystals, iridium crystals were observed as single-phase inclusions within fresh Mg-chromite crystals (Fig. 8 #10–11) and rarely form a binary phase with other PGM like Os-S (Fig. 8 #12). Osmium contents of osmium grains range from 47.33 to 61.06 wt.%, Ir contents are from 37.0 to 43.13 wt.%, and Ru concentrations are from 0.89 to 11.8 wt.% (Table 3). Iridium, Os and Ru contents of the iridium grains are 41.3–73.45 wt.%, 24.36–35.11 wt.% and <4.55 wt.%, respectively (Table 3). Iridium grains within the samples PK50-2-1 and PK55-1 have Pd contents of 1.6 wt.% and 6.0 wt.%, respectively (Table 3).

In chromitite sample PK26-1, in addition to laurite and osmium, sperrylite was detected in association with laurite (Fig. 8 #6). It contains 57.24 wt.% Pt and 42.36 wt.% As; small amounts of Os (0.20 wt.%), Ru (0.25 wt.%) and Rh (0.12 wt.%) contribute the mineral composition (Table 3). Next to the laurite-sperrylite association, a very small (~2 μm) irarsite phase was also detected (Fig. 8 #6).

Three unknown phases were also detected within fresh Mg-chromite crystals. These were euhedral, single-phase and about 2 μm in size (Fig. 8 #13–#15). Phase Un#1 is enriched in PGE, with Os, Ir, Ru and Rh contents of 43.65 wt.%, 11.87 wt.%, 9.68 wt.% and 1.28 wt.%, respectively. S content of the phase is 32.08 wt.%, and Pd and Fe concentrations are 0.16 wt.% and 0.13 wt.%, respectively (Table 3). The chemical formula of this phase (Un#1) is $(Os, Ru, Ir, Rh, Fe, Pd)_2S_5$. Un#2 and Un#3 phases differ from Un#1 in that Os is absent, Ir is enriched, and the Ni and Cu base metals are present (Table 3). More specifically, Un#2 contains 50.93 wt.% Ir, 8.03 wt.% Rh, 1.13 wt.% Ni, 9.24 wt.% Cu and 24.82 wt.% S, while Un#3 contains 44.28 wt.% Ir, 17.5 wt.% Rh, 6.49 wt.% Ni, 6.43 wt.% Cu and 20.53 wt.% S (Table 3). The chemical formulas of these phases are $Ir(Rh, Pt, Ni, Cu)S_3$ for Un#2 and $(Ir, Rh, Ru)_2(Ni, Cu)S_3$ for Un#3.

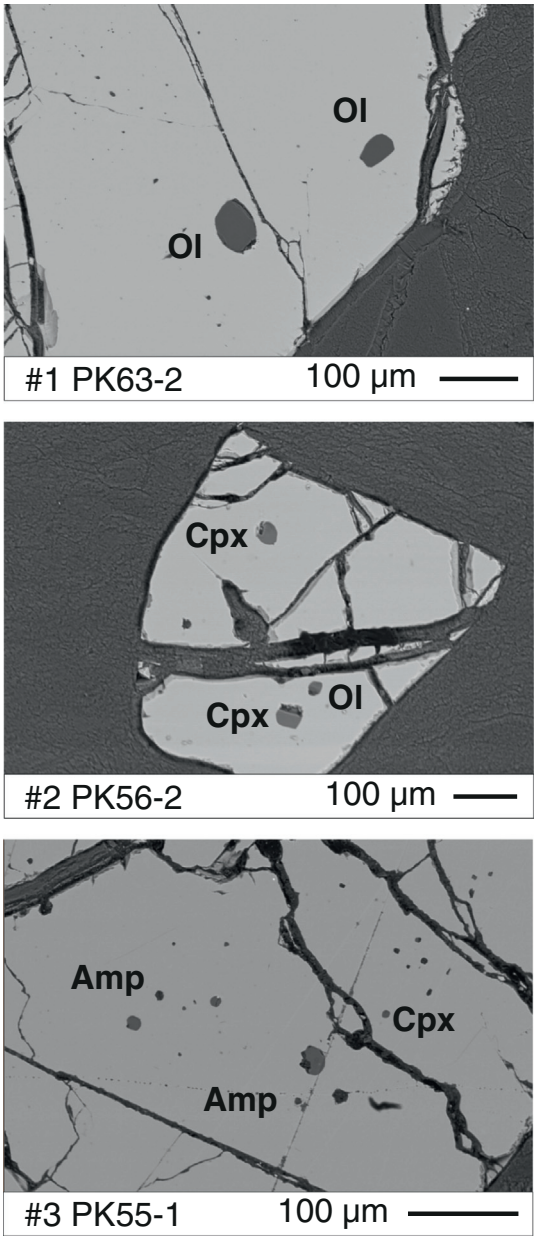

Fig. 10. BSE images showing primary silicate inclusions in Mg-chromites from the Kızılyüksek chromitites. Ol: Olivine; Cpx: Clinopyroxene; Amp: Amphibole.

Table 4
Average composition of olivine (Ol), clinopyroxene (Cpx) and amphibole (Amp) inclusions in Mg–chromites from each chromitite sample. Mg#, Fo = 100 × Mg / (Mg + Fe^{2+}), Wo = 100 × Ca / (Ca + Mg + Fe^{2+}), En = 100 × Mg / (Ca + Mg + Fe^{2+}), Fs = 100 × Fe / (Ca + Mg + Fe^{2+}), N: Number of spot analysis, bdl: below detection limit.

Sample#	PK4-1	PK50B	PK50-2-1	PK50-2-2	PK55-1	PK56-2	PK63-2	PK4-1	PK15	PK50B	PK50-2-1	PK56	PK56-2	PK63-2	PK15	PK50-2-1	PK55-1
N	6	9	3	5	5	2	5	3	2	2	3	5	30	4	2	1	16
Mineral	Ol	Ol	Ol	Ol	Ol	Ol	Ol	Cpx	Cpx	Cpx	Cpx	Cpx	Cpx	Cpx	Amp	Amp	Amp
SiO_2	41.54	42.82	41.14	41.85	42.38	42.94	41.26	53.21	55.19	55.77	51.77	53.36	54.82	53.76	45.98	43.01	45.68
TiO_2	bdl	bdl	bdl	bdl	bdl	bdl	bdl	0.04	0.09	bdl	0.06	0.07	0.06	bdl	0.41	0.36	0.42
Al_2O_3	bdl	bdl	bdl	bdl	bdl	bdl	bdl	0.80	1.26	0.78	2.83	1.30	0.85	1.23	10.80	12.17	10.49
Cr_2O_3	0.79	0.79	0.93	0.76	0.78	0.40	0.80	1.57	1.42	1.84	1.56	1.81	1.66	1.55	3.63	3.96	3.58
FeO	4.39	3.15	3.23	3.06	3.52	3.14	3.33	1.43	1.13	1.09	0.99	1.15	1.14	1.26	1.79	2.06	1.84
MnO	bdl	bdl	bdl	bdl	bdl	bdl	bdl	bdl	bdl	bdl	bdl	bdl	bdl	bdl	bdl	bdl	bdl
NiO	0.48	0.63	0.62	0.68	0.56	0.66	0.56	bdl	bdl	bdl	bdl	bdl	bdl	bdl	0.15	bdl	bdl
MgO	50.34	52.89	50.86	51.23	54.71	54.68	50.53	17.06	17.32	16.81	16.61	16.99	17.36	17.25	19.10	18.76	20.30
CaO	bdl	0.09	0.07	0.08	bdl	0.10	bdl	24.52	23.97	25.09	24.37	24.76	24.93	24.22	12.73	12.48	12.61
Na_2O	bdl	bdl	bdl	bdl	bdl	bdl	bdl	0.24	0.31	0.33	0.31	0.38	0.39	0.30	3.71	4.30	3.21
K_2O	bdl	bdl	bdl	bdl	bdl	bdl	bdl	bdl	0.27	bdl	bdl	bdl	bdl	bdl	0.09	0.16	0.05
∑	97.54	100.37	96.84	97.67	101.96	101.91	96.48	98.86	100.97	101.72	98.49	99.83	101.21	99.57	98.38	97.25	98.18
Si	1.019	1.015	1.013	1.020	0.993	1.004	1.019	1.960	1.979	1.989	1.912	1.947	1.968	1.960	6.474	6.179	6.436
Ti	0.000	0.000	0.000	0.000	0.000	0.000	0.000	0.001	0.002	0.000	0.002	0.002	0.002	0.000	0.043	0.039	0.045
Al	0.000	0.000	0.000	0.000	0.000	0.000	0.000	0.035	0.053	0.033	0.123	0.056	0.036	0.053	1.792	2.060	1.742
Cr	0.015	0.015	0.018	0.015	0.014	0.007	0.016	0.046	0.040	0.052	0.046	0.052	0.047	0.045	0.404	0.449	0.399
Fe^{2+}	0.090	0.063	0.066	0.062	0.069	0.061	0.069	0.044	0.034	0.033	0.030	0.035	0.034	0.038	0.211	0.248	0.216
Mn	0.000	0.000	0.000	0.000	0.000	0.000	0.000	0.000	0.000	0.000	0.000	0.000	0.000	0.000	0.000	0.000	0.000
Ni	0.009	0.012	0.012	0.013	0.011	0.012	0.011	0.000	0.000	0.000	0.000	0.000	0.000	0.000	0.017	0.000	0.000
Mg	1.840	1.870	1.867	1.861	1.912	1.905	1.859	0.937	0.926	0.893	0.915	0.924	0.929	0.938	4.009	4.018	4.264
Ca	0.000	0.002	0.002	0.002	0.000	0.002	0.000	0.968	0.921	0.958	0.964	0.968	0.959	0.946	1.920	1.921	1.903
Na	0.000	0.000	0.000	0.000	0.000	0.000	0.000	0.017	0.022	0.023	0.022	0.027	0.027	0.021	1.013	1.197	0.878
K	0.000	0.000	0.000	0.000	0.000	0.000	0.000	0.000	0.012	0.000	0.000	0.000	0.000	0.000	0.016	0.028	0.010
∑	2.974	2.977	2.978	2.973	2.999	2.993	2.974	4.007	3.989	3.980	4.013	4.011	4.002	4.002	15.899	16.139	15.892
Fo	95	97	97	97	97	97	96										
Mg#								95	97	97	97	96	96	96	95	94	95
Wo	–	–	–	–	–	–	–	49.7	49.0	50.9	50.5	50.2	49.9	49.2	–	–	–
En	–	–	–	–	–	–	–	48.1	49.2	47.4	47.9	48.0	48.3	48.8	–	–	–
Fs	–	–	–	–	–	–	–	2.3	1.8	1.7	1.6	1.8	1.8	2.0	–	–	–

5.4.2. Silicate mineral inclusions

Primary inclusions of olivine, clinopyroxene and amphibole, <100 μm in size, occur within Mg-chromite crystals (Fig. 10). Table 4 shows average chemical composition of silicate inclusions from each sample. Olivine compositions range between Fo_{95} and Fo_{97}. Their NiO content is relatively high (0.48–0.68 wt.%), and Cr_2O_3 concentrations range between 0.40 and 0.93 wt.% (Table 4). Clinopyroxenes, which are the most common silicate inclusion in Kızılyüksek chromitites (Fig. 10 #2), are mostly diopside in composition, with the Wo, En and Fs contents ranging between 49.0 and 50.9%, 47.4–49.2% and 1.6–2.3%, respectively (Table 4). The Al_2O_3 concentrations of the clinopyroxenes are 0.78 to 2.83 wt.%, and TiO_2 contents are very low, mostly <0.1 wt.%. Their Cr_2O_3 contents range between 1.42 and 1.84 wt.%. In addition to olivine and clinopyroxene inclusions, amphibole inclusions were also detected (Fig. 10 #3). Amphibole inclusions are represented by high Mg# values (~95), and their Cr_2O_3 and Na_2O contents are 3.58–3.96 wt.% and 3.21–4.30 wt.%, respectively. Amphiboles with very low TiO_2 contents (0.36–0.42 wt.%) also have low K_2O contents (<0.17 wt.%) (Table 4). Considering the International Mineralogical Association (IMA) classification criteria, amphibole inclusions in Mg-chromite crystals of Kızılyüksek chromitites are of calcic character (Ca >1.50 apfu and Na + K > 0.50 apfu) and *pargasite-edenite* composition.

5.4.3. Base metal minerals (BMM) inclusions

In Kızılyüksek chromitites, in addition to PGM and silicate inclusions, primary BMS inclusions were detected. BMM also occur as secondary phases in fractures and cracks within the silicate matrix. In Mg-chromite crystals, primary inclusions of heazlewoodite, 5–10 μm in size, contain 70.29–72.66 wt.% Ni, 0.44–1.15 wt.% Fe, and 26.25–27.83 wt.%S; the As concentration is <0.28 wt.% (Table 5). Euhedral primary pentlandite inclusions are very small (<4 μm), and only one pentlandite crystal could be quantitatively analysed. Ni and Fe contents of this pentlandite grain are 29.80 wt.% and 27.65 wt.%, respectively (Table 5). Awaruite grains, which are thought to form by alteration of BMM inclusions, are generally associated with fractures and cracks within Mg-chromite crystals and contain 0.72 wt.% Cu.

6. Discussion

6.1. Parental melt composition in equilibrium with Kızılyüksek chromitites

According to Maurel and Maurel (1982), the Al_2O_3 content of the melt that crystallizes the chromitites is represented by the empirical equation $(Al_2O_3)_{spinel} = 0.035 \times (Al_2O_3)^{2.42}$ which is based on the observation that the Al_2O_3 contents in Cr-spinel is a function of Al_2O_3 contents in melt. Also, Maurel (1984) proposed the following formula to determine the FeO/MgO ratio of the melt that crystallizes the most massive chromitites, in which the Fe–Mg exchange between silicate matrix and chromite crystals is the lowest:

$$\mathrm{Ln(FeO/MgO)_{chromite}} = 0.47 - 1.07\mathrm{Al\#_{chromite}} + 0.64\mathrm{Fe^{3+}\#_{chromite}} + \mathrm{Ln(FeO/MgO)_{melt}}$$

$$\mathrm{Al\#} = \mathrm{Al}/\left(\mathrm{Al} + \mathrm{Cr} + \mathrm{Fe^{3+}}\right) \text{ and } \mathrm{Fe^{3+}\#} = \mathrm{Fe^{3+}}/\left(\mathrm{Al} + \mathrm{Cr} + \mathrm{Fe^{3+}}\right)$$

Kamenetsky et al. (2001) studied Cr-spinel crystals in volcanic rocks from the mid-ocean ridge (MOR), island arc (Arc) and within plate settings and determined the Al_2O_3 and TiO_2 contents of the melt inclusions in these crystals. Kamenetsky et al. (2001) also established the relationship between the Al_2O_3 and TiO_2 contents of melt inclusions and the Cr-spinel crystals that contain these inclusions and stated that the chemical character of the melt crystallizing the Cr-spinel can be estimated using the chemistry of Cr-spinels. Rollinson (2008) used Kamenetsky et al.'s (2001) data set on Cr-spinels and melt inclusions of volcanic rocks from various tectonic settings and proposed two different equations for various tectonic settings (Arc and MOR), assessing the relationship

Table 5
Representative electron microprobe analyses of primary (Hzl, Pn) and secondary (Aw) BMMs in Mg–chromites of the Kızılyüksek chromitites. Hzl: Heazlewoodite, Aw: Awaruite, Pn: Pentlandite, bdl: below detection limit.

Sample#	PK15	PK15	PK15	PK63-2	PK49B	PK49B	PK49B
Inclusion#	1	3	4	1	2c	2a	2b
Mineral	Hzl	Hzl	Hzl	Hzl	Pn	Aw	Aw
Ni	70.59	70.29	72.66	71.64	39.80	75.51	75.85
Fe	0.44	1.08	0.98	1.15	29.65	23.14	22.76
Cu	bdl	0.03	bdl	bdl	0.04	0.68	0.72
S	26.70	27.06	27.83	26.25	28.49	bdl	bdl
As	0.28	0.16	bdl	0.27	0.03	0.20	0.15
∑	98.00	98.63	101.47	99.31	98.00	99.53	99.47
Ni	2.976	2.943	2.956	2.937	4.550	3.006	3.019
Fe	0.020	0.051	0.042	0.049	4.437	0.968	0.952
Cu	0.000	0.001	0.000	0.000	0.005	0.025	0.027
∑metal	3.000	3.000	3.000	2.986	9.000	4.000	4.000
S	1.991	1.994	2.000	1.970	7.996	0.000	0.000
As	0.009	0.006	0.000	0.009	0.004	0.000	0.000
∑anion	2.000	2.000	2.000	1.979	8.000	0.000	0.000
∑	5.000	5.000	5.000	5.000	17.000	4.000	4.000

between the Al_2O_3 and TiO_2 contents of such Cr-spinel crystals and melt inclusions.

The aforementioned equations, based on the Al_2O_3 and TiO_2 values of Cr-spinel, have been used often to explain the character of the primary melt that crystallizes the Cr-spinel and to determine the tectonic setting of podiform chromitites (Mondal et al., 2006; Mukherjee et al., 2010, 2015; Uysal et al., 2007b; Rollinson, 2008; Page and Barnes, 2009; González-Jiménez et al., 2011; Zaccarini et al., 2011; Rollinson and Adetunji, 2013; Akmaz et al., 2014; Zhou et al., 2014; Uysal et al., 2015).

In this study, using these equations, the primary composition of the melts that crystallized the Kızılyüksek chromitites was determined. The Kızılyüksek chromitites are disseminated, massive, banded and nodular-textured, and only massive samples, for which the Fe-Mg exchange between silicate matrix and chromite crystals is the lowest, were used to determine the FeO/MgO ratio of the melt. The FeO/MgO ratio of the melt that crystallized the Kızılyüksek chromitites was in the range of 0.56–0.85, which is within the range or even lower than those proposed for boninitic melts (0.7–1.4; Wilson, 1989) (Table 7). Melt FeO/MgO values estimated for the studied chromitites are within the range of those suggested for Muğla (southwestern Turkey) high-Cr chromitites (FeO/MgO: 0.3–1.1; Uysal et al., 2009a), which was thought to have crystallized from boninitic melt.

For most studied chromitite samples, the Cr# values of the Mg-chromite crystals are above 70, and Fe^{2+}# and Ti contents indicate that these chromitites were formed from a boninitic melt in a subduction zone setting (Fig. 12). Considering that the studied chromitites were derived from a melt in a subduction setting, the following equations proposed by Rollinson (2008) for the arc setting were used to determine the Al_2O_3 and TiO_2 contents of the melt that crystallized the Kızılyüksek chromitites.

$$Al_2O_{3(melt)} = 5.2181 Ln(Al_2O_3)_{Cr-spinel} - 1.0505$$

$$TiO_{2(melt)} = 1.0963 \times TiO_{2(Cr-spinel)}^{0.7863}$$

The calculated Al_2O_3 and TiO_2 contents of the melt were estimated to be 10.67–13.74 wt.% and 0.19–0.44 wt.%, respectively (Fig. 13).

Melt Al_2O_3 and TiO_2 values calculated for the Kızılyüksek chromitites show similarity to high-Cr chromitites in Oman ophiolite (Oman), Thetford Mines ophiolite (Canada), Sagua de Tanamo ophiolite (Eastern Cuba), Loubusa ophiolite (China), Kahramanmaraş, Malatya and Gaziantep (Southeastern Turkey), Orhaneli and Harmancık ophiolites (Bursa) and Muğla ophiolite (southwestern Turkey) (Table 7). The high-Cr chromitites in these regions were thought to have crystallized from melts of boninite character in a subduction zone, as were the Kızılyüksek chromitites.

Table 6
PGE concentrations (ppb) of the Kızılyüksek chromitites and related values. Primitive mantle values are from McDonough and Sun (1995). bdl: below detection limit.

Element	Os	Ir	Ru	Rh	Pt	Pd	Pd/Ir	Rh_N/Os_N	ΣIPGE	ΣPPGE	ΣPGE	$PPGE_N/IPGE_N$
Primitive Mantle	3.4	3.2	5.0	0.9	7.1	3.9	1.22		11.6	11.9	23.5	
Detection Limits	2	2	2	1	2	2						
PK6	14	16	28	6	3	bdl	–	1.62	58	9	67	0.34
PK7	22	26	64	8	4	2	0.08	1.37	112	14	126	0.26
PK15	9	15	32	6	6	3	0.20	2.52	56	15	71	0.45
PK21	19	19	35	5	36	14	0.74	0.99	73	55	128	0.70
PK22	27	33	80	9	10	3	0.09	1.26	140	22	162	0.26
PK25	4	7	12	3	3	3	0.43	2.83	23	9	32	0.61
PK26	31	38	72	10	5	3	0.08	1.22	141	18	159	0.26
PK37	9	25	37	11	3	bdl	–	4.62	71	14	85	0.49
PK49	21	28	34	7	bdl	2	0.07	1.26	83	9	92	0.27
PK50	10	21	36	10	6	bdl	–	3.78	67	16	83	0.51
PK56	19	22	40	6	2	bdl	–	1.19	81	8	89	0.24
PK63	16	23	34	7	2	bdl	–	1.65	73	9	82	0.30
PK64	6	11	24	9	bdl	3	0.27	5.67	41	12	53	0.76
PK65	4	9	27	9	bdl	bdl	–	8.50	40	9	49	0.71

Table 7
Calculated parental melt composition of the Kızılyüksek chromitites, some high–Cr chromitites from all over the world and parental melt composition of Cr–spinels in bonitite and MORB.

Location/ophiolite	Al_2O_3	TiO_2	FeO/MgO	References
Kızılyüksek (Adana/Turkey)	10.7–13.7	0.19–0.44	0.56–0.85	This study
Orhaneli (Bursa/Turkey)	10.0–10.9	0.23–0.43		Uysal et al., 2015
Harmancık (Bursa/Turkey)	10.5–11.0	0.23–0.28		Uysal et al., 2015
Southeast Turkey	10.2–11.9	0.17–0.39		Akmaz et al., 2014
Muğla (Southwest Turkey)	8.8–10.5		0.3–1.1	Uysal et al., 2009a
Luobusa (China)	13.8	0.31	0.97	Zhou et al., 2014
Sagua de Tanamo (East Cuba)	12.9–14.2	0.22–0.39	0.9–1.5	González-Jiménez et al., 2011
Thetford Mines (Canada)	9.3–13.0	0.12–0.30		Page and Barnes, 2009
Oman	11.8–12.9	0.23–0.34		Rollinson, 2008
Boninite	10.6–14.4		0.7–1.4	Wilson, 1989
MORB	16		1.2–1.6	Wilson, 1989

6.2. Crystallization conditions of the Kızılyüksek chromitites

6.2.1. Implications from solid inclusions (PGM, BMM and silicate) in Mg-chromite

The textural characteristics of mineral inclusions within the Cr-spinel crystals provide information about the origin of these phases. Euhedral/subhedral silicate, PGM and BMM inclusions in unaltered Cr-spinel crystals indicate that these inclusions are of magmatic origin and were crystallized prior to or simultaneously with the Cr-spinel (Prichard and Tarkian, 1988; Garuti et al., 1999; Brenan and Andrews, 2001; Uysal et al., 2005; Uysal et al., 2007a; Uysal, 2008; Akmaz et al., 2014).

Platinum-group elements in chromitites generally occur as alloys and sulfide phases, and PGM paragenesis is used as an indicator for establishing temperature (T) and sulfur fugacity [$f(S_2)$] of the melt that crystallized the PGM and thus chromitites (Augé, 1985; Ahmed and Arai, 2003; Ahmed, 2007; Uysal et al., 2007a, 2015; Uysal, 2008; González-Jiménez et al., 2011, 2014; Zaccarini et al., 2011; Kapsiotis et al., 2011; Akmaz et al., 2014). To determine T and $f(S_2)$ conditions of the melt from which the PGM in the Cr-spinel crystals were crystallized, Brenan and Andrews (2001) and Bockrath et al. (2004) carried out experimental studies. The authors observed that laurite with a composition close to that of pure RuS_2 was crystallized from a melt under high temperature (1200–1300 °C) and low sulfur fugacity [$\log f(S_2) = -2$ to -1], and that with decreased temperature and increased $f(S_2)$, the Ru in laurite is partly replaced by Os; as a result, Os-rich laurite is crystallized. Therefore, there is a general consensus that PGM, thought to be crystallized prior to or simultaneously with the Cr-spinel crystals, are crystallized from the primary melt in the order of IPGE alloys, Ru-rich laurite and Os-rich laurite (Westland, 1981; Stockman and Hlava, 1984; Brenan and Andrews, 2001; Bockrath et al., 2004; Distler et al., 2008).

In the Kızılyüksek chromitites, the presence of Os and Ir alloys and Ru-rich laurites (Ru# = ~0.97) might indicate that the chromitites were formed at relatively higher temperature and low $f(S_2)$ conditions (Fig. 14). However, the Ru# values of laurite grains decrease from 0.97 to 0.72, showing that temperature of the melt from which the chromitites crystallized was decreased and $f(S_2)$ value was relatively increased. In addition, the absence of erlichmanite in PGM paragenesis of Kızılyüksek chromitites implies that the temperature decrease during the Mg-chromite crystallization was limited.

Sperrylite has been observed within the fractures and cracks of Cr-spinel crystals or as a hydrothermal alteration product within the silicate matrix (Tarkian and Prichard, 1987; Prichard and Tarkian, 1988; Augé et al., 2002; Ahmed, 2007) and has rarely been recorded as a phase of magmatic origin (Augé et al., 2002). Augé et al. (2002) stated that sperrylite in chromitites could be of both magmatic and hydrothermal origin. Augé et al. (2002) also affirmed that sperrylite occurs simultaneously with the hydrothermal alteration product laurite and that these laurites contain much more As (1.01–5.97 wt.%) compared to magmatic laurites. Laurite and sperrylite phases in sample PK26-1 from the Kızılyüksek chromitites occur as an inclusion within the Mg-chromite crystal (Fig. 8 #6), forming a binary phase, and As content of the laurite is <0.88 wt.%. This indicates that sperrylite occurring simultaneously with laurite is of magmatic origin, and concentrations of

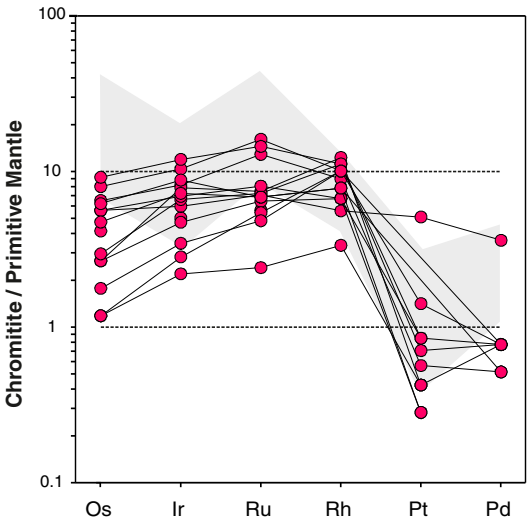

Fig. 11. Primitive mantle-normalized PGE patterns for the Kızılyüksek chromitites. Grey field indicates PGE patterns of chromitites in the mantle peridotites from all over the world. The data source for this field is taken from Page et al., 1982; Bacuta et al., 1990; Bonavia et al., 1993; Yang and Seccombe, 1993; Augé and Maurizot, 1995; Leblanc, 1995; Graham et al., 1996; Zhou et al., 1996, 1998; Uçurum et al., 2000, 2006; Uysal, 2007; Uysal et al., 2005, 2007a, 2007b, 2009a; Prichard et al., 2008.

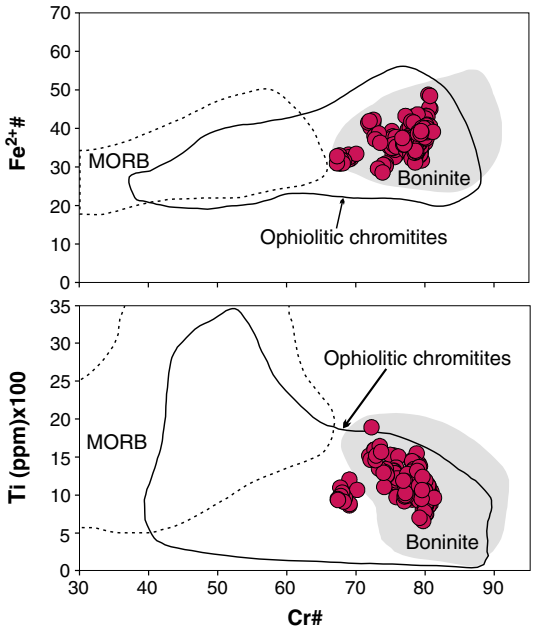

Fig. 12. Diagrams of Ti (ppm) versus Cr# (a) and Cr# versus Fe^{2+}# (b) of Mg-chromite grains from the Kızılyüksek chromitites showing possible tectonic setting of the chromitites. Boninite, MORB and podiform chromitites fields are from Page and Barnes (2009).

elemental Pt and As in the melt were sufficient to crystallize the sperrylite.

Primary inclusions of heazlewoodite within the Mg-chromite crystals are not associated with hydrothermal processes, but instead indicate a magmatic origin. Heazlewoodite inclusions that are texturally shown to have crystallized prior to or simultaneously with Cr-spinel are important for explaining the physicohemical conditions under which Cr-spinel is crystallized. However, heazlewoodite is a mineral that can crystallize within a wide range of T and fS_2 conditions (Stockman and Hlava, 1984). Therefore, these minerals occurring as primary inclusions within Mg-chromite crystals may not yield reliable information regarding the temperature and fS_2 conditions of Mg-chromite crystallization. The presence of primary inclusions of Ru-rich laurites within the Kızılyüksek chromitites allows the determination of a narrow range of T and fS_2 conditions. Such paragenesis indicates that these inclusions were crystallized at temperatures of about 1200–1300 °C and fS_2 conditions ranging from log −2 to log −1 (Fig. 14).

The type of primary silicate inclusions within Cr-spinel crystals also yields important information about the hydrous/anhydrous character of the melt that crystallized these inclusions. Moreover, the abundance of incompatible trace element contents of silicate inclusions in Cr-spinels also provides valuable data on the source of the melt that crystallized the chromitites. TiO_2 contents of the clinopyroxenes, which are the most abundant silicate inclusion within the Kızılyüksek chromitites, are quite low (TiO_2 < 0.1 wt.%). Saka et al. (2014) pointed out that the mantle peridotites hosting the Kızılyüksek chromitites are the residue of at least two stages of partial melting. They stated that the mantle peridotites that formed the Pozantı-Karsantı ophiolite are thought to have been slightly depleted as a result of a low degree of partial melting in a mid-ocean ridge environment. Then, due to the change in the tectonic regime, they were later remelted and depleted in a supra-subduction zone (SSZ). Therefore, it was proposed that the rocks forming the crustal part of the Pozantı-Karsantı ophiolite were formed from melts that originated due to melting of formerly depleted mantle in subduction zone. Considering that the Kızılyüksek chromitites were formed from a boninitic melt in a subduction environment (Fig. 12), that the mantle material to be melted in the subduction setting was already depleted (particularly the incompatible Na and K elements), and that the degree of partial melting in the subduction environment is relatively high, it is expected that Na and K content of the resulting melt would be depleted. Therefore, Na and K contents of the clinopyroxene inclusions within the Cr-spinel crystals originating from such a melt should also be depleted. The clinopyroxene inclusions within the Mg-chromite crystals that make up the Kızılyüksek chromitites contain low Na_2O (0.24 to 0.39 wt.%) and K_2O (usually below detection limit) contents, and support the idea that the melt that crystallized the chromitites originated from high-degree partial melting of a depleted source.

According to Lorand and Ceuleneer (1989), amphibole minerals in Cr-spinel crystals are crystallized from a hydrous melt in a subduction environment, and subducting oceanic lithosphere is the melt source. Former studies have confirmed these assertions (McElduff and Stumpfl, 1991; Uysal et al., 2009b; González-Jiménez et al., 2011; Zhou et al., 2014). Therefore, the presence of primary amphibole inclusions within the Kızılyüksek ophiolitic chromitites is indicative of crystallization from a hydrous melt in a subduction environment.

6.2.2. Magmatic fractionation

Results of in-situ (LA-ICPMS) trace element analysis conducted on a limited number of chromitite samples (total of 9 point analysis from 3 chromitite samples) show that the Mg-chromite crystals in samples PK59B and PK20 have similar Ga, Mg, Co, Mn and Cr concentrations, slightly enhanced Al contents, and relatively depleted Ni, Fe and V contents compared to Cr-spinels from boninites. The Mg-chromite crystals in these chromitite samples show a significant anomaly for Ti with respect to Cr-spinel crystals in boninites (Fig. 6). It is a fact that melt that crystallized chromitites at greater depths is less differentiated compared to melts that crystallize the boninites. Although the partition of very little Ti into the Cr-spinel ($D_{Ti}^{spinel/melt}$ ~ 0.048; McKenzie and O'Nions, 1991) during the formation of chromitites results in a slight decrease in the Ti content of the melt, the absence of Ti containing silicate or different oxide phases crystallization together with the Cr-spinel crystallization will give rise to relatively increased Ti concentration in the residual melt. Titanium contents of chromitites associated with cumulate dunites that originated from differentiated melts following chromitite crystallization in the deeper mantle might also depend on the amount of Cr-spinels and Ti-bearing silicate and oxide phases crystallization. Significant positive Ti anomalies in the Mg-chromite crystals of two of the samples (PK20, PK59B; Fig. 6) may indicate that Cr-spinel crystallization was not accompanied by Ti-bearing phases. Significant V enrichment in the Cr-spinel crystals of the boninites compared to levels seen in samples PK59B and PK20 might support the idea that the melt that crystallized the boninites was much more differentiated than the melt that crystallized the investigated chromitites (Fig. 6). Another chromitite sample (PK26B) shows substantial enrichment of Al, Ga and Ti compared to the Cr-spinel crystals in the boninites, but does not show any positive Ti anomaly. On the other hand, the Co and Mn contents are depleted with respect to the Cr-spinel crystals in the

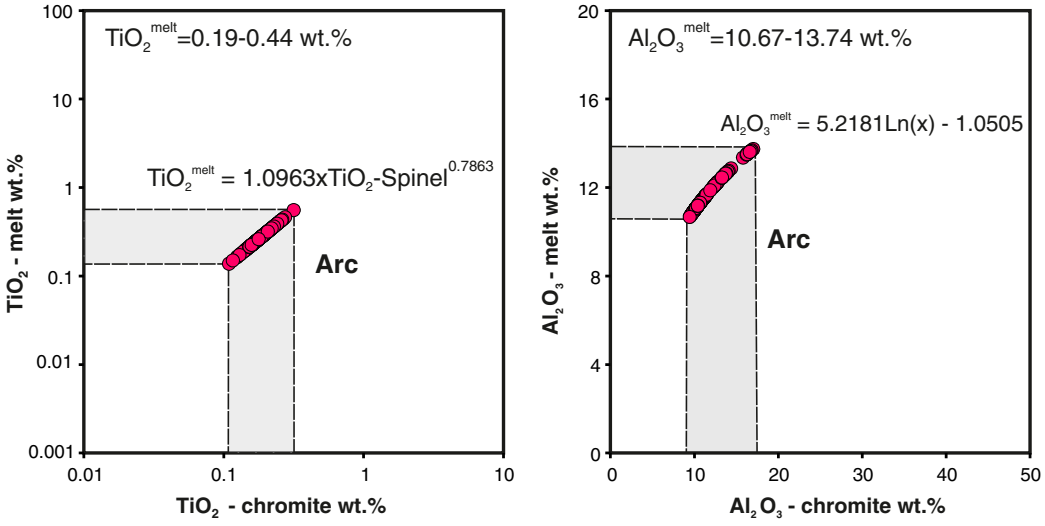

Fig. 13. Plots of calculated Al_2O_3 (wt.%) and TiO_2 (wt.%) contents of the parental melts in equilibrium with the Kızılyüksek chromitites.

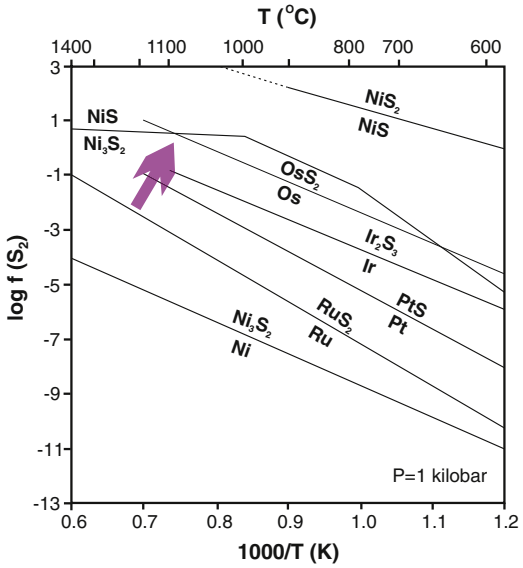

Fig. 14. Diagram of metal-sulfide equilibrium lines (Stockman and Hlava, 1984). The yellow arrow indicates the proposed crystallization trend of fS_2-T for the Kızılyüksek chromitites. (For interpretation of the references to color in this figure legend, the reader is referred to the web version of this article.)

boninites and the other samples, and the V content is enriched compared to samples PK59B and PK20 (Fig. 6). This shows that the melt that crystallized this sample was much more differentiated than the melts that crystallized the other chromite samples. The negative relationship between the Ga and Co concentrations and the Cr# values of the Mg-chromite crystals (Fig. 7) supports Mg-chromite formation from a differentiating melt (Page and Barnes, 2009). Regarding major and trace element compositions, the Mg-chromite crystals resemble the Cr-spinel crystals that form the Caribou Mountain Block (CMB; Page and Barnes, 2009) chromitites, which were thought to have been created in a subduction zone setting (Fig. 6).

Platinum-group elements known to be rather chalcophile and siderophile are mostly present in the core of the Earth, with very low concentrations seen in the Earth's mantle. Platinum-group elements having various melting temperatures are retained by several sulfide phases in the mantle and are incorporated into the melts depending on the degree of partial melting in the mantle (Zhou et al., 1998; Prichard et al., 2008; González-Jiménez et al., 2011). The degree of partial melting in mid-ocean ridges is in the range of 2–15% (Beard et al., 2007; Hellebrand et al., 2001; Uysal et al., 2012, 2014, 2015); low-degree partial melting in such environments results in the transfer of PPGE in sulfide phases with lower melting temperature to the melt formed and noteworthy depletion of such elements in mantle rocks (Barnes et al., 1985; Leblanc, 1991). A higher degree of partial melting is required to remove IPGE in the monosulfide solid solution (Mss) from the mantle rocks (e.g., Alard et al. 2000; Lorand and Alard, 2001).

It has been proposed that the mantle rocks of the Pozantı-Karsantı ophiolite are residues of at least two stages of partial melting. According to Saka et al. (2014), these rocks first underwent low-degree partial melting in the MOR environment and were then remelted in a subduction setting, resulting in the mantle rocks being remnants of a high-degree partial melting. Hydrous remelting of highly PPGE depleted first stage melting residue in a subduction zone, giving rise to formation of PPGE-depleted and IPGE-enriched melt. Therefore, chromitites thought to be crystallized from such melts are expected to be enriched in IPGE and depleted in PPGE. Osmium-iridium alloys and then Ru-rich laurite minerals are first expected to be crystallized from IPGE-rich melts, followed by crystallization of the erlichmanite and BMM phases with a decrease in temperature and increase in $f(S_2)$ (Brenan and Andrews, 2001; Bockrath et al., 2004; González-Jiménez et al., 2011; Uysal et al., 2015). Such crystallization is observed as inclusions within the Cr–spinel crystals of ophiolitic chromitites. PGM paragenesis of the chromitites defines total PGE contents. The Kızılyüksek chromitites, which are thought to be derived from a boninitic melt, are relatively depleted in PGE (32–162 ppb) compared to other chromitites in Turkey.

In a primitive mantle-normalized PGE diagram, the Kızılyüksek chromitite samples can be seen to be partly depleted in Os compared to chromitites across the globe (Fig. 11). The Ru-rich character of most laurites in the Kızılyüksek chromitites and the predominance of laurite minerals over osmium minerals indicate that the melt that crystallized these chromitites was Os-poor. The Os-depletion of these chromitites can be explained by two possible scenarios.

1. *Crystallization of chromitites from a relatively differentiated melt*: In such a case, chromitites that were previously crystallized from such melts (and possibly in a deeper mantle) are expected to be Os-richer and contain much more osmium alloys.
2. *Depletion of Os in partially molten mantle*: The mantle, which is the source of the melts from which the chromitites were crystallized, may have been depleted in Os as a result of a previous high-degree partial melting. However, in such a case, the concentrations of Ir and Ru, which are more incompatible than Os, would be expected to be more depleted. In the primitive mantle-normalized diagram (Fig. 11), the Ir and Ru contents of the studied chromitites are higher than Os, which may rule out this hypothesis. Therefore, the somewhat low Os concentrations in the Kızılyüksek chromitites might imply that the melt that crystallized these chromitites was differentiated.

In the case of crystallization from a basaltic melt, Os leaves the melt by incorporating into first crystallizing phases, such as Os-Ir alloys or laurite crystals. The more incompatible Rh element, however, probably remains in the melt. Thus, the Rh/Os ratios of the chromitites would become low, and in the PGE diagrams, negative trends from Os to Rh and Pd for the ophiolitic chromitites would be expected. The Rh/Os ratios of these chromitites may reflect the degree of differentiation of the melt that crystallized the chromitites. For the Kızılyüksek chromitites, the primitive mantle-normalized Rh/Os ratios range from 0.99 to 8.5, indicating that the melts that crystallized these chromitites were differentiated to varying degrees. Considering that these chromitites were crystallized from differentiated melts, the chromitite Rh/Os ratios would be expected to increase with decreasing Cr-spinel Cr# values. The absence of such a relationship in the Kızılyüksek chromitites indicates that these chromitites were not crystallized from a single melt but rather from melts originating from various sections of mantle at different depths.

6.3. Conclusions

Different models and tectonic settings have been proposed for the formation of chromitites. Lago et al. (1982) first suggested that chromitites are formed by the accumulation of chromite crystals in the basaltic melts circulated within fractures of mantle rock in extensional zones. They also stated that dunite peripheries develop around the chromitites as a result of the melt-peridotite interaction. The rock-melt interaction is another model proposed for chromitite formation (Arai and Yurimoto, 1994) that has been widely used. In this model, harzburgite depleted in the MOR tectonic environment interacts with basaltic melt in the subduction zones, and the orthopyroxene in harzburgite are consumed by the melt. As a result of this interaction, the melt is gradually enriched in SiO_2, and Cr-spinel starts to crystallize. Mixing between silicate melt and fluids in subduction zones is another proposed mechanism for the crystallization of nodular chromitites (Matveev and Ballhaus, 2002).

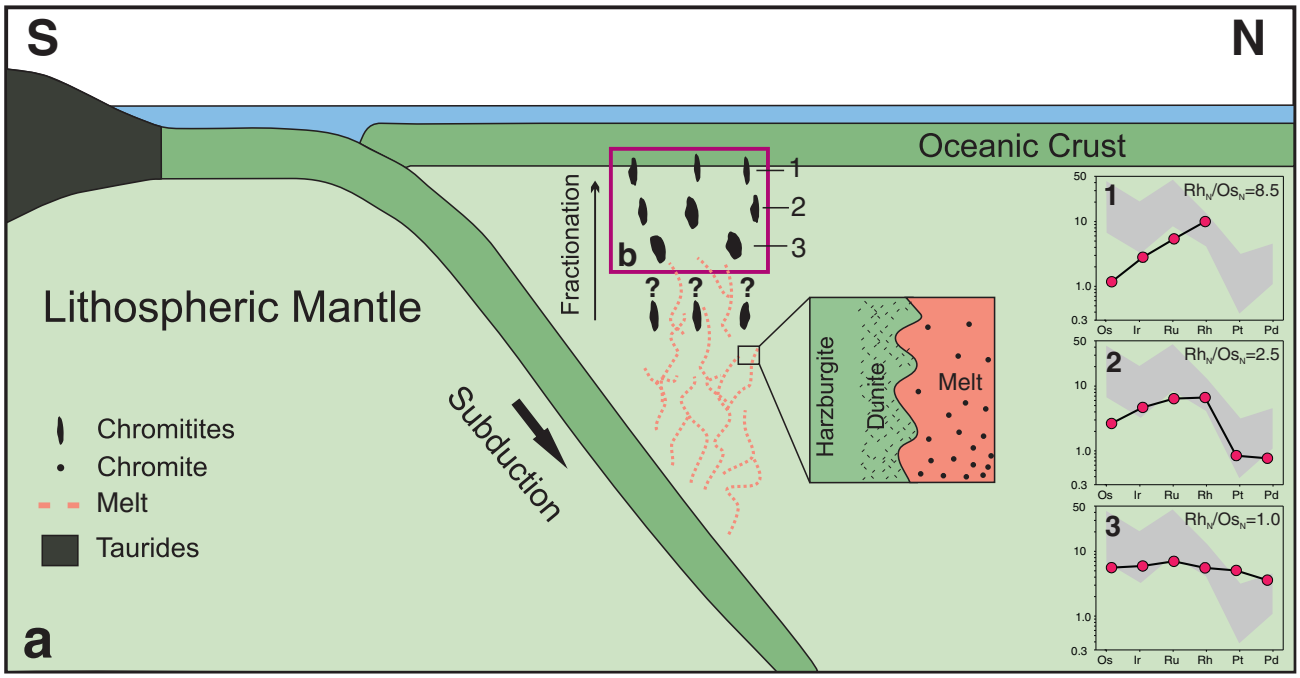

Fig. 15. Proposed tectonic model for the formation of the Kızılyüksek ophiolitic chromitites.

Different tectonic settings have also been proposed for chromitite formation. For instance, high-Cr chromitites are thought to be formed from boninitic type melts in subduction zones, while high-Al chromitites are crystallized from MORB type melts in back arc basins (Zhou and Robinson, 1994). The presence of primary clinopyroxene inclusions with low TiO_2 contents and amphibole inclusions (hydrous silicate) in the Mg-chromite crystals in our study indicates that the Kızılyüksek chromitites were formed in a subduction zone from melts originating from high-degree partial melting (Fig. 15a). This is confirmed by Saka et al.'s (2014) findings that the mantle peridotites of the ophiolitic sequence making up the Kızılyüksek chromitites are the residue of high-degree partial melting.

TiO_2 and Al_2O_3 contents of the melts that crystallized the Kızılyüksek chromitites indicate crystallization from a boninite-type melt. In the Kızılyüksek chromitites, the degree of IPGE enrichment is higher than that of PPGE, showing that the melts that generated the chromitites were previously depleted in PPGE and that the IPGE were separated from the mantle by a high-degree melting process in a subduction zone. Moreover, depletion of Os compared to Ir and Ru in the Kızılyüksek chromitites might indicate that they were crystallized from variably differentiated boninitic melts (Fig. 15b).

Acknowledgements

This paper is based on part of Erdi Avcı's Master thesis, and has been funded by TUBITAK project (#109Y219). We are very grateful to Utku Bağcı and E. Yalçın Ersoy for their help during the field studies. Melanie Kaliwoda, Rupert Hochleitner and Dirk Müller are acknowledged for their great help with the electron microprobe measurements. Thomas Aiglsperger and Kurtuluş Günay are thanked for their scientific contribution which improved the paper. We thank Guest editor Sisir Mondal and Editor-in-Chief Franco Pirajno for their scientific contribution and handling of our paper.

References

Ahmed, 2007. Diversity of platinum–group minerals in podiform chromitites of the late Proterozoic ophiolite, Eastern Desert, genetic implications. Ore Geol. Rev. 32, 1–19.

Ahmed, A.H., Arai, S., 2002. Unexpectedly high–PGE chromitite from the deeper mantle section of the Northern Oman ophiolite and its tectonic implications. Contrib. Mineral. Petrol. 143, 263–278.

Ahmed, A.H., Arai, S., 2003. Platinum–group minerals in podiform chromitites of the Oman ophiolite. Can. Mineral. 41, 597–616.

Ahmed, A.H., Arai, S., Abdel-Aziz, Y.M., Ikenne, M., Rahimi, A., 2009. Platinum–group elements distribution and spinel composition in podiform chromitites and associated rocks from the upper mantle section of the Neoproterozoic Bou Azzer ophiolite, Anti–Atlas, Morocco. J. Afr. Earth Sci. 55, 92–104.

Akmaz, R.M., Uysal, İ., Saka, S., 2014. Compositional variations of chromite and solid inclusions in ophiolitic chromitites from the southeastern Turkey: implications for chromitite genesis. Ore Geol. Rev. 58, 208–224.

Alard, O., Griffin, W.L., Lorand, J.P., 2000. Non-chondritic distribution of the highly siderophile elements in mantle sulphides. Nature 407, 891–894.

Arai, S., 1997. Origin of podiform chromitites. J. Asian Earth Sci. 15, 303–310.

Arai, S., Yurimoto, H., 1994. Podiform chromitites of the Tari–Misaka ultramafic complex, Southwestern Japan, as mantle–melt interaction products. Econ. Geol. 89, 1279–1288.

Augé, T., 1985. Platinum–group mineral inclusions in ophiolitic chromitite from the vourinos complex, Greece. Can. Mineral. 23, 163–171.

Augé, T., Maurizot, P., 1995. Stratiform and alluvial platinum mineralization in the New Caledonia ophiolite complex. Can. Mineral. 33, 1023–1045.

Augé, T., Salpeteur, I., Bailly, L., 2002. Magmatic and hydrothermal platinum–group minerals and base–metal sulfides in the Baula complex, India. Can. Mineral. 40, 277–309.

Bacuta, G.C., Kay, R.W., Gibbs, A.K., Lipin, B.R., 1990. Platinum–group element abundance and distribution in chromite deposits of the Acoje Block, Zambales ophiolite complex, Philippines. J. Geochem. Explor. 37, 113–145.

Barnes, S.J., Naldrett, A.J., Gorton, M.P., 1985. The origin of the fractionation of the platinum–group elements in terrestrial magmas. Chem. Geol. 53, 303–323.

Beard, A.D., Downes, H., Mason, P.R.D., Vetrin, V.R., 2007. Depletion and enrichment processes in the lithospheric mantle beneath the Kola Peninsula (Russia): evidence from spinel lherzolites and wehrlite xenoliths. Lithos 94, 1–24.

Bingöl, A.F., 1978. Petrologie Du Masif Ophiolitique de Pozantı–Karsantı (Taurus Cilicien, Turquie): Etude de La Orientale, these 3′e Cycle. Universite Strasbourg.

Bockrath, C., Ballhaus, C., Holzheid, A., 2004. Stabilities of laurite RuS_2 and monosulfide liquid solution at magmatic temperature. Chem. Geol. 208, 265–271.

Bonavia, F.F., Diella, V., Ferrario, A., 1993. Precambrian podiform chromitites from Kenticha Hill, Southern Ethiopia. Econ. Geol. 88, 198–202.

Brenan, J.M., Andrews, D.R.A., 2001. High–temperature stability of laurite and Ru Os–Ir alloys and their role in PGE fractionation in mafic magmas. Can. Mineral. 39, 341–360.

Çakır, Ü., 1978. Petrologie Du Masisf De Pozantı–Karsantı (Taurus Cilicien, Turquie): Etude La Partie Centralla. These De Doctorat d'Ing Vol. 251. Univ. Strasbourg.

Çapan, U., 1980. Approach to Internal Structure, Petrology and Petrochemitsry of Ophiolitic Massifs in Touride Belt (Marmaris, Mersin, Pozantı, Pınarbaşı, Ve Divriği) (PhD Thesis) H.Ü., Graduate School of Natural and Applied Sciences, Ankara/Turkey.

Çataklı, A.S., 1978. Petrographie et Geochimie des Filons de la Partie Occidentale du Masif Ophiolitique de Pozantı–Karsantı (Turqie), 6 eme R.A.S.T. Orsay, Paris, p. 94.

Chan, T.K., Finch, I.J., 2001. Determination of platinum-group elements and gold by inductively coupled plasma mass spectrometry. Australian Platinum Conference. Perth, Western Australia.
Dick, H.J.B., Bullen, T., 1984. Chromian spinel as a petrogenetic indicator in abyssal and alpine–type peridotites and spatially associated lavas. Contrib. Mineral. Petrol. 86, 54–76.
Dilek, Y., Moores, E.M., Panayiotou, A., 1990. Regional tectonics of the Eastern Mediterrranean ophiolites. In: Malpas, J., Moores, E., Xenophontos, C. (Eds.), Ophiolites–Oceanic Crustal Analogues. Proc Troodos Ophiolite Symp. Geological Survey Cyprus 1987, pp. 295–309.
Dinter, D.A., 1988. Late Cenozoic extension of the Alpine collisional orogen, Northestern Greece: origin of the North Aegean Basin. Geol. Soc. Am. Bull. 110, 1208–1230.
Distler, V.V., Kryachko, V.V., Yudovskaya, M.A., 2008. Ore petrology of chromite–PGE mineralization in the Kempirsai ophiolite complex. Mineral. Petrol. 92, 31–58.
El Ghorfi, M., Melcher, F., Oberthür, T., Boukhari, A.E., Maacha, L., Maddi, A., Mhaili, M., 2008. Platinum group minerals in podiform chromitites of Bou Azzer ophiolite, Anti Atlas, Central Morocco. Mineral. Petrol. 92, 59–80.
Ferrario, A., Garuti, G., 1988. Platinum-group minerals in chromite-rich horizons of the Niquelandia Complex (Central Goias, Brazil). In: Prichard, H.M., Potts, P.J., Bowels, J.F.W., Cribb, S.J. (Eds.), GeoPlatinum 87. Elsevier Applied Sciences, London and New York, pp. 261–272.
Fischer, W., Amossé, J., Leblanc, M., 1988. PGE distribution in some ultramafic rocks and minerals from the Bou Azzer ophiolitic complex (Morocco). In: Prichard, H.M., Potts, P.J., Bowles, J.F.W., Cribb, S.J. (Eds.), Geo-Platinum-87. Elsevier Applied Sciences, London and New York, pp. 199–210.
Garuti, G., Zaccarini, F., Moloshag, V., Alimov, V., 1999. Platinum–group minerals as indicators of sulfur fugacity in ophiolitic upper mantle: an example from chromitites of the Ray–Iz ultramafic complex, Polar Urals, Russia. Can. Mineral. 37, 1099–1115.
Garuti, G., Pushkarev, V.E., Thalhammer, O.A.R., Zaccarini, F., 2012. Chromitites of the urals (part 1): overview of chromite mineral chemistry and geo–tectonic setting. Ofioliti 37 (1), 27–53.
González-Jiménez, J.M., Proenza, J.A., Gervilla, F., Melgarejo, J.C., Blanco-Moreno, J.A., Ruiz-Sanchez, R., Griffin, W.L., 2011. High–Cr and high–Al chromitites from the Sagua de Tanamo District, Mayari–Cristal ophiolitic massif (Eastern Cuba): constraints on their origin from mineralogy and geochemistry of chromian spinel and platinum group elements. Lithos 125, 101–121.
González-Jiménez, J.M., Griffin, W.L., Gervilla, F., Proenza, J.A., O'Reilly, S.Y., Pearson, N.J., 2014. Chromitites in ophiolites: how, where, when, why?, part 1. A review and new ideas on the origin and significance of platinum–group minerals. Lithos 189, 127–139.
Graham, I.T., Franklin, B.J., Marshall, B., 1996. Chemistry and mineralogy of podiform chromitite deposits, Southern NSW, Australia: a guide to their origin and evolution. Mineral. Petrol. 37, 129–150.
Hellebrand, E., Snow, J.E., Dick, H.J.B., Hofmann, A.W., 2001. Coupled major and trace elements as indicators of the extent of melting in mid–ocean–ridge peridotites. Nature 410, 677–681.
Juteau, T., 1979. Ophiolites des Taurides: Essai sur leur historie oceanique. Revue de Geologie Dynamique de Geographic Physique 21 (3), 191–214 Paris.
Juteau, T., 1980. Ophiolites of Turkey. Ofioliti 2, 199–237.
Kamenetsky, V.S., Crawford, A.J., Meffre, S., 2001. Factors controlling chemistry of magmatic spinel: an empirical study of associated olivine, Cr–spinel and melt inclusions from primitive rocks. J. Petrol. 42, 655–671.
Kapsiotis, A., Grammatikopoulos, A.T., Tsikouras, B., Hatzipanagiotou, K., Zaccarini, F., Garuti, G., 2011. Mineralogy, composition and PGM of chromitites from Pefki, Pindos ophiolite complex (NW Greece): evidence for progressively elevated *f*As conditions in the upper mantle sequence. Mineral. Petrol. 101, 129–150.
Lago, B., Rabinowicz, M., Nicolas, A., 1982. Podiform Cromite ore bodies, a genetic model. J. Petrol. 23, 103–125.
Leblanc, M., 1991. Platinum–group glements and gold in Gphiolitic complexes: distribution and fractionation from mantle to oceanic floor. In: Petters, T.J., Nicolas, A., Coleman, R. (Eds.), Ophiolite Genesis and Evolution of the Oceanic Lithosphere 5. Ministry of Petroleum and Minerals, Sultanate of Oman, pp. 231–260.
Leblanc, M., 1995. Chromitite and ultramafic rock compositional zoning through a paleotransform fault, Poum, New Caledonia. Econ. Geol. 90, 2028–2039.
Leblanc, M., Ceuleneer, G., 1992. Chromite crystallization in a multicellular magma flow, evidence from a chromitite dike in the Oman ophiolite. Lithos 27, 231–257.
Leblanc, M., Violette, J.F., 1983. Distribution of aluminum-rich and chromium–rich chromite pods in ophiolite peridotites. Econ. Geol. 78, 293–301.
Lorand, J.P., Ceuleneer, G., 1989. Silicate and base–metal sulfide inclusions in chromites from the Maqsad area (Oman ophiolite, gulf of Oman): a model for entrapment. Lithos 22, 173–190.
Lorand, J.-P., Alard, O., 2001. Platinum-group element abundances in the upper mantle: new constraints from in situ and whole-rock analyses of Massif Central xenoliths (France). Geochim Cosmochim Acta 65, 2789–2806.
Matveev, S., Ballhaus, C., 2002. Role of water in the origin of podiform chromitite deposits. Earth Planet. Sci. Lett. 203, 235–243.
Maurel, C., 1984. Etude Expérimentale de L'équilibre Spinelle Chromifere Liquide Silicate Basique, SFMC Meet., "Les spinelles", Lille.
Maurel, C., Maurel, P., 1982. Etude Experimentale de la Distribbution de L'aluminium Entre Bain Silicate Basique et Spinelle Chromifere, Implications Petrogenetiques, Teneur en Chrome Des Spinelles. Bull. Mineral. 105, 197–202.
McDonough, W.F., Sun, S.S., 1995. The composition of the earth. Chem. Geol. 120, 223–253.
McElduff, B., Stumpfl, E.E., 1991. The chromite deposits of the Troodos complex, Cyprus–evidence for the role of a fluid phase accompanying chromite formation. Mineral. Deposita 26, 307–318.
McKenzie, D., O'Nions, R.K., 1991. Partial melt distributions from inversion of rare earth element concentrations. J. Petrol. 32, 1021–1091.
Mondal, S., Ripley, E., Li, C., Frei, R., 2006. The genesis of archaean chromitites from the Nuasahi and Sukinda massifs in the Singhbhum Craton, India. Precambrian Res. 148, 45–66.
MTA (General Directrorate of Mineral Research and Exploration), 2002. 1:500.000 scaledGeological Maps of Turkey (Adana map section), Ankara-Turkey.
Mukherjee, R., Mondal, S.D., Rosing, M.T., Frei, R., 2010. Compositional variations in the Mesoarchean chromites of the Nuggighalli schist belt, Western Dharwar Craton (India): potential parental melts and implications for tectonic setting. Contrib. Mineral. Petrol. 160, 865–885.
Mukherjee, R., Mondal, S.K., González-Jiménez, J.M., Griffin, W.L., Pearson, N.J., 2015. Trace-element fingerprints of chromite, magnetite and sulfides from the 3.1 Ga ultramafic–mafic rocks of the Nuggihalli greenstone belt, Western Dharwar craton (India). Contributions to Mineralogy and Petrology 169, 1–23.
Okay, A.I., 2008. Geology of Turkey: a synopsis. Anschnitt 21, 19–42.
Orberger, B., Friedrich, G.H., Woermann, E., 1988. Platinum-group element mineralization in the ultramafic sequence of the Acoje Ophiolite block, Zambales, Philippines. In: Prichard, H.M., Potts, P.J., Bowels, J.F.W., Cribb, S.J. (Eds.), GeoPlatinum 87. Elsevier Applied Sciences, London and New York, pp. 361–379.
Page, P., Barnes, S.-J., 2009. Using trace elements in chromites to constrain the origin of podiform chromitites in the Thetford Mines Ophiolite. Quebec, Canada. Econ Geol. 104, 997–1018.
Page, N.J., Pallister, J.S., Brown, M.A., Smewing, J.R., Haffty, J., 1982. Palladium, platinum, rhodium, ruthenium and iridium in chromite rich rocks from the Semail ophiolite, Oman. Can. Mineral. 20, 537–548.
Prichard, M.H., Tarkian, M., 1988. Platinum and palladium minerals from two PGE–rich localities in the Shetland ophiolite complex. Can. Mineral. 26, 979–990.
Prichard, H.M., Neary, C.R., Fisher, F.C., O'Hara, M.J., 2008. PGE–rich podiform chromitites in the Al'Ays ophiolite complex, Saudi Arabia: an example of critical mantle melting to extract and concentrate PGE. Econ. Geol. 103, 1507–1529.
Rollinson, H., 2008. The geochemistry of mantle chromitites from the northern part of the Oman ophiolite: inferred parental melt composition. Contrib. Mineral. Petrol. 156, 273–288.
Rollinson, H., Adetunji, J., 2013. The geochemistry and oxidation state of Fodiform chromitites from the mantle section of the Oman ophiolite: a review. Gondwana Res. 27, 543–554.
Saka, S., Uysal, İ., Akmaz, R.M., Kaliwoda, M., Hochleitner, R., 2014. The effects of partial melting, melt–mantle interaction and fractionation on ophiolite generation: constraints from the late cretaceous Pozantı–Karsantı ophiolite, southern Turkey. Lithos 202–203, 300–316.
Stevens, R.E., 1944. Composition of some chromites of the western hemisphere. Am. Mineral. 29, 1–34.
Stockman, H.W., Hlava, P.F., 1984. Platinum–group minerals in alpine chromitites from Southwestern Oregon. Econ. Geol. 79, 491–508.
Tarkian, M., Prichard, H.M., 1987. Irarsite–Hollingworthite solid–solution series and other associated Ru–, Os–, Ir–, and Rh–bearing PGM's from the Shetland ophiolite complex. Mineral. Deposita 22, 178–184.
Tekeli, O., 1981. Properties of ophiolitic melange in Taurides. Geological Bulletin of Turkey 24, 57–64.
Tekeli, O., Aksay, A., Ürgün, B.M., Işık, A., 1984. Geology of the Aladağ Mountains. In: Tekeli, O., Göncüoğlu, M.C. (Eds.), Geology of the Taurus Belt. MTA, pp. 143–158.
Uçurum, A., Lechler, P.J., Larson, L.T., 2000. Platinum–group element distribution in chromite ores from ophiolite complexes, Western Turkey. Trans. Inst. Min. Metall. (Sect B: Appl. Earth Sci.) 109, 112–120.
Uçurum, A., Koptagel, O., Lechler, P.J., 2006. Main–component geochemistry and platinum–group–element potential of Turkish chromite deposits, WITH emphasis on the Mugla Area. Int. Geol. Rev. 48, 241–254.
Uysal, İ., 2007. Muğla (GB–Türkiye) Petrology of Upper Mantle Peridotites and Ophiolitic Chromitites: Mineral Chemistry, Major Oxide–Trace Element–REE–PGE Geochemistry, PGE Mineralogy and Re–Os Isotobes (PhD thesis) K.T.Ü., Graduate School of Natural and Applied Sciences, Trabzon/Turkey.
Uysal, İ., 2008. Platinum–group minerals (PGM) and other solid inclusions in the Elbistan–Kahramanmaraş, mantle–hosted ophiolitic chromitites, South–Eastern Turkey: their petrogenetic significance. Turk. J. Earth Sci. 17, 729–740.
Uysal, İ., Sadiklar, M.B., Tarkian, M., Karsli, O., Aydin, F., 2005. Mineralogy and composition of the chromitites and their platinum–group minerals from Ortaca (Muğla SW Turkey): evidence for ophiolitic chromitite genesis. Mineral. Petrol. 83, 219–242.
Uysal, İ., Tarkian, M., Sadiklar, M.B., Şen, C., 2007a. Platinum–group–elements geochemistry and mineralogy in ophiolitic chromitites from the Kop Mountains, Nourtheastern Turkey. Can. Mineral. 45, 355–377.
Uysal, İ., Zaccarini, F., Garuti, G., Meisel, T., Tarkian, M., Bernhardt, H.J., Sadiklar, M.B., 2007b. Ophiolitic chromitites from the Kahramanmaras area, southeastern Turkey: their platinum–group elements (PGE) geochemistry, mineralogy and Os–isotope signature. Ofioliti 32, 151–161.
Uysal, İ., Tarkian, M., Sadiklar, M.B., Zaccarini, F., Meisel, T., Garuti, G., Heidrich, S., 2009a. Petrology of Al– and Cr–rich ophiolitic chromitites from the Muğla, SW Turkey: implications from composition of chromite, solid inclusions of platinum–group mineral, silicate, and base–metal mineral, and Os–isotope geochemistry. Contrib. Mineral. Petrol. 158, 659–674.
Uysal, İ., Zaccarini, F., Sadıklar, M.B., Tarkian, M., Thalhammer, O.A.R., Garuti, G., 2009b. The podiform chromitites in the Dağküplü and Kavak mines, Eskişehir ophiolite (NW–Turkey): genetic implications of mineralogical and geochemical data. Geol. Acta 7 (3), 351–362.
Uysal, İ., Ersoy, Y., Karslı, O., Dilek, Y., Sadıklar, M.B., Ottley, C.J., Tiepolo, M., Meisel, T., 2012. Coexistence of abyssal and ultra–depleted SSZ type mantle peridotites in a neo–Tethyan ophiolite in SW Turkey: constrains from mineral

composition, wholerock geochemistry (major–trace–REE–PGE) and Re–Os isotope systematics. Lithos 132–133, 50–69.
Uysal, İ., Şen, A.D., Ersoy, E.Y., Dilek, Y., Saka, S., Zaccarini, F., Escayola, M., Karsli, O., 2014. Geochemical make–up of oceanic peridotites from NW Turkey and the multi–stage melting history of the Tethyan upper mantle. Mineral. Petrol. 108, 49–69.
Uysal, İ., Akmaz, R.M., Kapsiotis, A., Demir, Y., Saka, S., Avcı, E., Müller, D., 2015. Genesis and geodynamic significance of chromitites from the Orhaneli and Harmancık ophiolites (Bursa, NWTurkey) as evidenced by mineralogical and compositional data. Ore Geol. Rev. 65, 26–41.
Westland, A.D., 1981. Inorganic chemistry of platinum group elements. In: Cabri, L.J. (Ed.), Platinum–Group Elements: Mineralogy, Geology, Recovery. Can. Inst. Mining Metall. Spec. 23, pp. 7–17.
Wilson, M., 1989. Igneous Petrogenesis. Unwin Hyman, London (466 pp.).
Yang, K., Seccombe, P.K., 1993. Platinum–group minerals in the chromitites from the great Serpentinite Belt, NSW, Australia. Mineral. Petrol. 47, 263–286.
Zaccarini, F., Garuti, G., Proenza, A.J., Thalhammer, O.A.R., Aiglsperger, T., Lewis, J.F., 2011. Chromite and platinum group elements mineralization in the Santa Elena ultramafic nappe (Costa Rica): geodynamic implications. Geol. Acta 9, 407–423.
Zhou, M.F., Robinson, P.T., 1994. High–chromium and high–aluminium podiform chromitites, Western China, relationship to partial melting and melt/rock interaction in the upper mantle. Int. Geol. Rev. 36, 678–686.
Zhou, M.F., Robinson, P.T., Malpas, J., Li, Z., 1996. Podiform chromitites in the Luobusa ophiolite (southern Tibet), implications for melt–rock interaction and chromite segregation in the upper mantle. J. Petrol. 37, 3–21.
Zhou, M.F., Sun, M., Keays, R.R., Kerrich, R., 1998. Controls on platinum–group elemental distributions of podiform chromitites, a case study of high–Cr and high–Al chromitites from Chinese orogenic belts. Geochim. Cosmochim. Acta 62, 677–688.
Zhou, M.F., Robinson, P.T., Su, B.X., Gao, J.F., Li, J.W., Yang, J.S., Malpas, J., 2014. Compositions of chromite, associated minerals, and parental magmas of podiform chromite deposits: the role of slab contamination of asthenospheric melts in suprasubduction zone environments. Gondwana Res. 26, 262–283.